Whang et al. BMC Chemical Engineering (2019) 1:9
https://doi.org/10.1186/s42480-019-0007-7

BMC Chemical Engineering

REVIEW Open Access

Heterogeneous catalysts for catalytic CO_2 conversion into value-added chemicals

Ho Seok Whang, Jinkyu Lim, Min Suk Choi, Jonghyeok Lee and Hyunjoo Lee*

Abstract

As climate change becomes increasingly evident, reducing greenhouse gases including CO_2 has received growing attention. Because CO_2 is thermodynamically very stable, its conversion into value-added chemicals such as CO, CH_4, or C_2H_4 is difficult, and developing efficient catalysts for CO_2 conversion is important work. CO_2 can be converted using the gas-phase reaction, liquid-phase reaction, photocatalytic reaction, or electrochemical reaction. The gas-phase reaction includes the dry reforming of methane using CO_2 and CH_4, or CO_2 hydrogenation using CO_2 and H_2. The liquid-phase reaction includes formic acid formation from pressurized CO_2 and H_2 in aqueous solution. The photocatalytic reaction is commonly known as artificial photo-synthesis, and produces chemicals from CO_2 and H_2O under light irradiation. The electrochemical reaction can produce chemicals from CO_2 and H_2O using electricity. In this review, the heterogeneous catalysts used for the gas-phase reaction or electrochemical reactions are discussed, because the liquid-phase reaction and photocatalytic reaction typically suffer from low productivity and poor durability. Because the gas-phase reaction requires a high reaction temperature of > 600 °C, obtaining good durability is important. The strategies for designing catalysts with good activity and durability will be introduced. Various materials have been tested for electrochemical conversion, and it has been shown that specific metals can produce specific products, such as Au or Ag for CO, Sn or Bi for formate, Cu for C_2H_4. Other unconventional catalysts for electrochemical CO_2 reduction are also introduced.

Keywords: Carbon dioxide, Dry reforming, Reverse water-shift reaction, Hydrogenation, Electrochemical reduction

Background

Global energy consumption has soared due to increasing population and industrialization, and anthropogenic CO_2 emissions have rapidly grown because the main energy resources being consumed today are fossil fuels. Increasing CO_2 concentration in the atmosphere is leading to global warming and a range of environmental problems. Global average temperatures have increased by 0.8 °C over the last 70 years [1]. International efforts have been proposed to reduce CO_2 emissions, such as the multinational Paris agreement. At the same time, many studies have focused on the development and application of renewable energy sources as a means of reducing dependence on fossil fuels [2, 3], as well as technologies for capturing and utilizing CO_2. CO_2 utilization would reduce greenhouse gases in the atmosphere and oceans where they can do harm, and CO_2 can also be used to produce valuable chemicals [4–6].

Because CO_2 is thermodynamically the most stable carbon species, its conversion into value-added products usually requires the expenditure of considerable energy. Various chemical processes have been reported that can convert CO_2 into chemicals such as CO, hydrocarbon, or oxygenated hydrocarbon. Gas-phase reaction, liquid-phase reaction, electrochemical, and photocatalytic reaction methods have been reported. Gas-phase reactions include the dry reforming of methane ($CH_4 + CO_2 \rightarrow 2CO + 2H_2$), CO_2 hydrogenation ($CO_2 + H_2 \rightarrow CO + H_2O$, which is also called the reverse water-gas shift reaction; $CO_2 + 4H_2 \rightarrow CH_4 + 2H_2O$). The liquid-phase reaction includes the production of formic acid using CO_2 dissolved in aqueous phase (CO_2 (aq) + H_2 (aq) → COOH). Several review papers about CO_2 hydrogenation can be found in the literatures [7–9]. However, CO_2 hydrogenation or formic acid formation requires H_2, which is mainly produced from

* Correspondence: azhyun@kaist.ac.kr
Department of Chemical and Biomolecular Engineering, Korea Advanced Institute of Science and Technology, Daejeon 34141, Republic of Korea

© The Author(s). 2019 **Open Access** This article is distributed under the terms of the Creative Commons Attribution 4.0 International License (http://creativecommons.org/licenses/by/4.0/), which permits unrestricted use, distribution, and reproduction in any medium, provided you give appropriate credit to the original author(s) and the source, provide a link to the Creative Commons license, and indicate if changes were made. The Creative Commons Public Domain Dedication waiver (http://creativecommons.org/publicdomain/zero/1.0/) applies to the data made available in this article, unless otherwise stated.

methane by steam reforming, which also produces a large amount of CO_2.

Electrochemical CO_2 reduction has received a great deal of attention recently, but the low solubility of CO_2 in aqueous solution has been a major obstacle. The use of a gas diffusion electrode has enabled the direct use of gaseous CO_2 for electrochemical conversion. This electrochemical conversion process does not require H_2 as a reactant. Photocatalytic CO_2 conversion also received growing attention because of its similarity to photosynthesis, but the process typically suffers from low productivity and poor stability.

Efficient catalysts can minimize the energy needed for reactions by reducing the activation energy. Various catalysts are being actively investigated to enhance CO_2 conversion and to control selectivity toward specific target products. In this review, we will focus on the heterogeneous catalysts for gas-phase CO_2 conversion and electrochemical CO_2 conversion. In the gas-phase CO_2 conversion, catalysts used for the dry forming of methane, CO_2 hydrogenation producing CO, and CO_2 hydrogenation producing CH_4 will be discussed. In the electrochemical CO_2 conversion, the specific catalysts used to produce CO, formic acid, and hydrocarbons will be discussed. Reviews of formic acid formation or photocatalytic CO_2 conversion can be found in the literature [10, 11].

Catalytic CO_2 conversion in gas phase

Dry reforming of methane

The dry reforming of methane (DRM) (Eq. (1)) can consume two greenhouse gases (CO_2 and CH_4) simultaneously and produce synthesis gas (abbreviated syn-gas, a mixture of CO and H_2). The ratio of H_2 to CO products is 1, which is much lower than other reforming reactions, such as the steam reforming of methane (SRM) and partial oxidation of methane (POM) (Eqs. (2) and (3)). The low ratio of H_2/CO is useful for synthesizing long chain hydrocarbons via the Fischer-Tropsch reaction [12–14].

$$CH_4 + CO_2 \rightarrow 2CO + 2H_2, \Delta H^\circ = 247\ \text{kJ mol}^{-1} \quad (1)$$

$$CH_4 + H_2O \rightarrow CO + 3H_2, \Delta H^\circ = 246\ \text{kJ mol}^{-1} \quad (2)$$

$$CH_4 + {}^{1}\!/_{2} O_2 \rightarrow CO + 2H_2, \Delta H^\circ = \text{-}36\ \text{kJ mol}^{-1} \quad (3)$$

The DRM reaction is endothermic, requiring a high reaction temperature of > 700 °C, which results in high energy cost [15, 16]. Figure 1 shows the DRM equilibrium plots at various temperatures and 1 atm [17]. The high temperature is required to attain high product yield. Side reactions such as the reverse water gas shift (RWGS) reaction (Eq. (4)) or carbon gasification reaction (Eq. (5)) can occur. The RWGS reaction affects the H_2/CO ratio; because the RWGS reaction happens more, the H_2/CO ratio decreases and CO_2 conversion increases. The steam produced from the RWGS reaction can react with carbon and produce syn-gas.

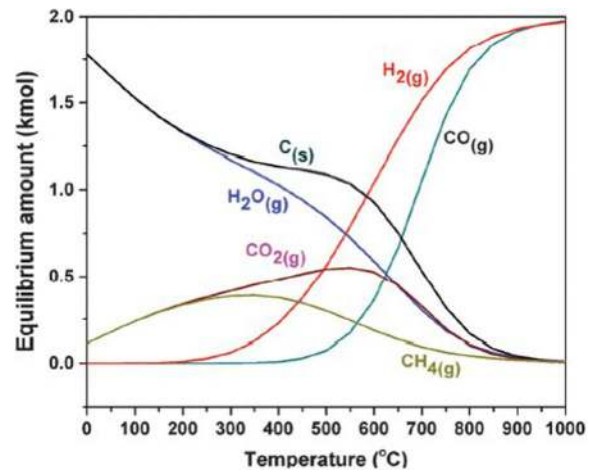

Fig. 1 Thermodynamic equilibrium plots for DRM at 1 atm, 0–1000 °C and at a reactant feed ratio of CO_2/CH_4 = 1. These equilibrium calculations were conducted using the Gibbs free energy minimization algorithm on HSC Chemistry 7.1 software. (Reprinted with permission from ref. [17]. Copyright 2013 Elsevier)

$$CO_2 + H_2 \rightarrow CO + H_2O, \Delta H^\circ = 41\ \text{kJ mol}^{-1} \quad (4)$$

$$C + H_2O \rightarrow CO + H_2, \Delta H^\circ = 131\ \text{kJ mol}^{-1} \quad (5)$$

Also, deactivation occurs easily due to sintering and coke deposition, which degrades long-term durability [12, 18–20]. Carbon is produced due to the Boudouard reaction and methane cracking (Eq. (6) and Eq. (7)). The carbon is thermodynamically the main product at temperatures lower than 570 °C [17]. DRM can proceed above 640 °C with methane cracking. The Boudouard reaction can't occur above 820 °C. Carbon can be produced by the Boudouard reaction, and methane cracking occurs from 570 to 700 °C [21]. Coke deposition is thermodynamically favored at low temperature. The carbon produced by methane cracking is likely to react with steam or carbon dioxide at high temperature. Thus, the DRM reaction should be performed at high temperature.

$$2CO + C \rightarrow C + CO_2, \Delta H^\circ = \text{-}172\ \text{kJ mol}^{-1} \quad (6)$$

$$CH_4 \rightarrow C + 2H_2, \Delta H^\circ = 75\ \text{kJ mol}^{-1} \quad (7)$$

Various heterogeneous catalysts have been developed, including metal supported catalysts, perovskites, and solid solution catalysts [22–26]. Precious metals (Pt, Rh

or Ru) are known to have high activity and durability, although at high price. Non-precious metals (Ni or Co) have been widely investigated as well. In this section, each component of DRM catalysts will be explained, and the strategies to enhance their activity and durability for DRM will be demonstrated.

Compositions of the catalysts: Metal, supports, promotors

Precious metals such as Pt, Rh and Ru are highly active for DRM and also resistant against coke deposition [27–30]. The precious metal-based catalysts show high activity in spite of the very small amount of metal catalyst used. For example, the Ru/ZrO_2-SiO_2 catalyst shows high activity and durability, as shown in Fig. 2, even though the Ru content was only 0.13 wt% [31].

Non-precious metals such as Ni or Co have been used more for DRM due to their cheap price and abundance [32–34]. Ni catalysts have shown a level of activity comparable to precious metals [30]. Alloyed metal catalysts are widely used for DRM because they have a different electronic structure than monometallic materials [35]. For example, the Ni-Fe alloy catalyst exhibited interesting behavior for DRM, as shown in Fig. 3. Monometallic Ni or Fe catalysts have shown poor durability, because the monometallic Ni catalyst is easily deactivated by coke deposition, and Fe is inactive for DRM. During the DRM reaction, the Ni-Fe alloy surface is partially oxidized; Ni maintains an oxidation state, while Fe is oxidized by CO_2. The oxidized FeO causes dealloying of the surface, and the FeO then oxidizes the carbon deposited on the surface, returning to Fe. The Fe^{2+}/Fe redox cycle plays a key role in enhancing durability in the DRM reaction [36].

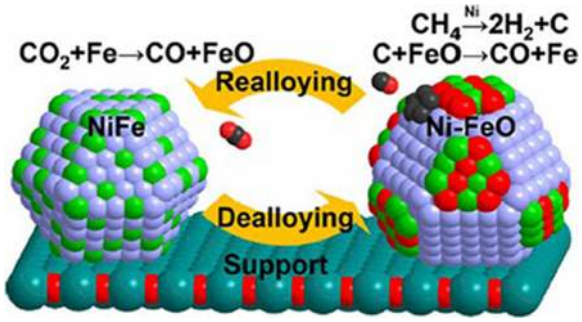

Fig. 3 Schematic diagram of the dealloying and realloying behavior of a Ni-Fe alloy particle during DRM. (Reprinted with permission from ref. [36]. Copyright 2017 American Chemical Society)

Supports can affect catalytic activity and durability for DRM [37]. The interaction between a support and metal can change the dispersion of the metal, resistance against sintering, and the electronic structure of the metal [28, 31]. Figure 4 shows the X-ray absorption fine structure (XAFS) analysis results of Rh catalysts deposited on various supports of Al_2O_3, TiO_2, etc. The X-ray absorption near edge structure (XANES) analysis in Fig. 4a shows that the Rh electronic structure has changed as a result of the support materials. TiO_2 supported Rh has a metallic character, while ɣ-Al_2O_3 supported Rh has an oxidic character. Figure 4b shows extended X-ray absorption fine structure (EXAFS) spectra. The Rh-Rh peak at 0.24 nm has different intensities with various supports. When the intensity is higher, the Rh-Rh coordination number is higher, indicating lower dispersion. The support materials affect the dispersion of the metal and chemical environment. [28].

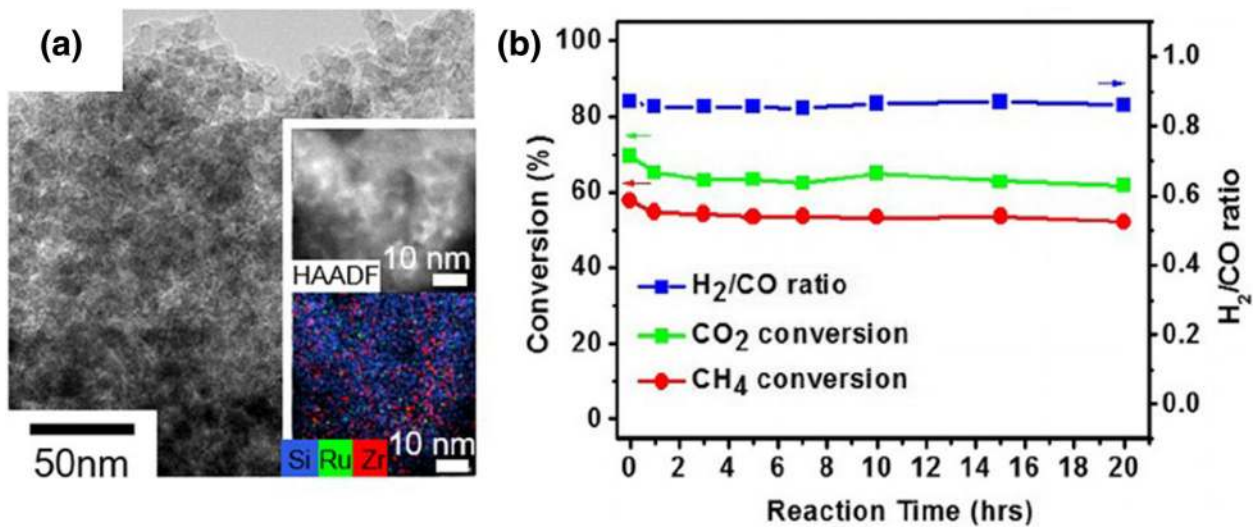

Fig. 2 a TEM images of fresh catalyst Ru/ZrO_2-SiO_2 catalyst; the insets indicate high angle annular dark field (HAADF)-scanning transmission electron microscope (STEM) images. **b** DRM results for a Ru-based catalyst with a space velocity of 80,000 ml/g_{cat}·h at 800 °C. (Reprinted with permission from ref. [31]. Copyright 2017 Elsevier)

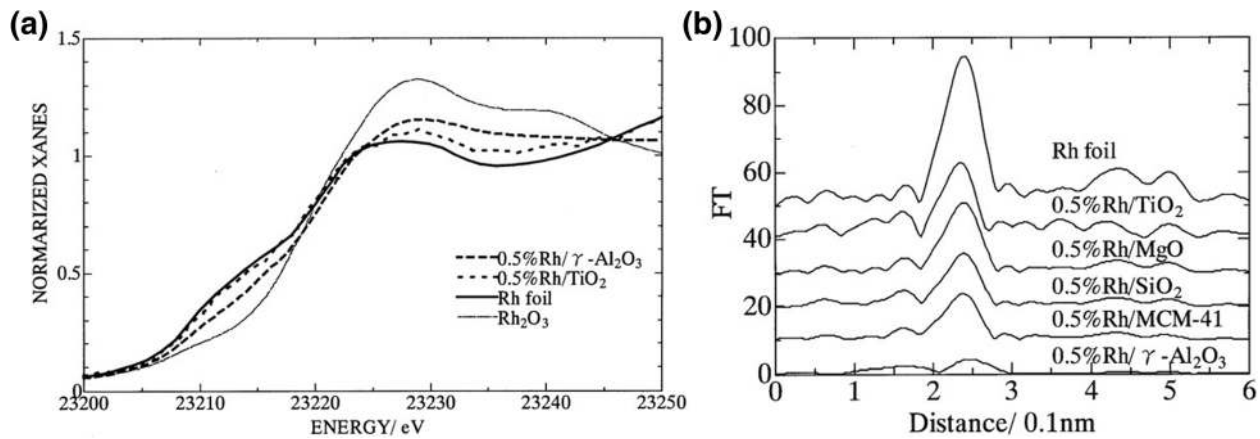

Fig. 4 Rh K-edge **a** XANES spectra and **b** EXAFS data for Rh catalysts deposited on various supports. (Reprinted with permission from ref. [28]. Copyright 2002 Springer)

The strong-metal support interaction (SMSI) causes a high dispersion of metals resulting in small sized metal nanoparticles with enhanced DRM activity. In addition, it increases resistance against sintering with enhanced durability [31, 38, 39]. The acidity and basicity of the support also affects catalytic properties. CO_2 is activated by forming formate with surface hydroxyl on an acidic support. CO_2 is activated by forming oxy-carbonate on a basic support. On an inert support such as SiO_2, both CO_2 and CH_4 are activated by metal with faster deactivation. A DRM catalyst supported on an inert material (SiO_2) is usually less active and less durable than on an acidic support (Al_2O_3) or basic support (La_2O_3) [23, 30, 40, 41].

Promoters have been widely used for DRM. Alkali metal oxides such as K_2O or CaO have been used to increase the basicity of the catalyst enhancing CO_2 adsorption [42–44]. CeO_2 or ZrO_2 were used to increase oxygen mobility [22, 45–50]. The transition between Ce^{3+} and Ce^{4+} can occur easily on CeO_2. The coke formed on Ni sites could be oxidized by using the redox cycle of CeO_2 with enhanced coke-resistivity [47]. The surface hydroxyl group can participate in the DRM surface reaction. Zhu et al. reported that the energy barrier for CH and C oxidation by surface OH was slightly lower than the barrier for surface O [51]. Ni et al. showed that the surface hydroxyl groups were increased by adding B_2O_3 to Ni catalyst, as shown in Fig. 5. The surface hydroxyl groups oxidize the carbon formed from methane decomposition, with enhanced resistance against coke deposition [52].

Coke-resistant catalysts

The key objective of catalysts developed for DRM is how to prevent coke deposition. Highly durable catalysts should avoid sintering because large Ni particles have severe coke formation at the surface, while small Ni nanoparticles do not have carbon deposition. In this section, various strategies to control the nano-structures of catalysts to prevent coke deposition will be discussed.

In order to prevent the sintering of nanoparticles, an inorganic oxide overlayer was formed on Ni nanoparticles [53–57]. As shown in Fig. 6, Ni nanoparticles with an average size of 5 nm were immobilized on SiO_2 spheres, then porous SiO_2 overlayers were formed on the Ni nanoparticles. The resulting Ni/SiO_2@SiO_2 catalyst showed high durability for DRM; activity was maintained for 170 h at 800 °C without Ni sintering [53].

Using this nano-structure, the effects of Ni size and support were evaluated independently. To evaluate the size effect, various sizes of Ni nanoparticles were deposited; 2.6, 5.2, 9.0, 17.3 nm. CH_4 turnover frequency clearly increased as Ni size decreased. The size effect could be evaluated exactly because the Ni size was barely changed even after the DRM reaction at 800 °C. The different metal oxide overlayers of Al_2O_3, MgO, ZrO_2, TiO_2, SiO_2 were formed on Ni/SiO_2 with a Ni particle size of 5.2 nm. The Al_2O_3 and MgO overlayers showed enhanced CH_4 turnover frequency, while the other overlayers hardly showed enhancement [55].

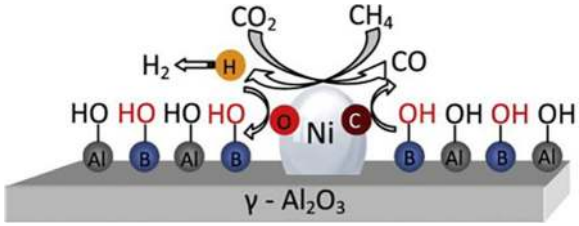

Fig. 5 Mechanism of carbon suppression on Ni/B_2O_3–Al_2O_3 catalyst. (Reprinted with permission from ref. [52]. Copyright 2012 Elsevier)

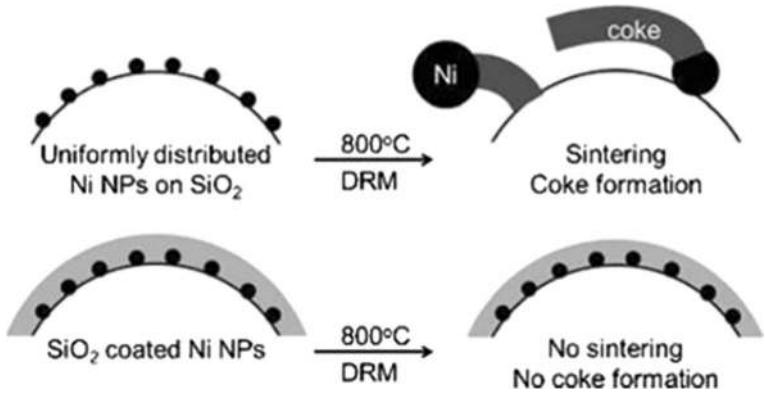

Fig. 6 Schematic illustration of Ni/SiO_2@SiO_2 catalyst with high coke resistance for the DRM reaction. (Reprinted with permission from ref. [53]. Copyright 2014 John Wiley and Sons)

Similarly, core-shell structures have been investigated; an outer shell such as SiO_2 separates the catalytic core material such as Ni nanoparticles while preventing sintering [58, 59]. The core-shell structures have been widely used in DRM, CO oxidation, and methane combustion reactions [60–62]. Li et al. developed a Ni yolk@Ni@SiO_2 catalyst, where a SiO_2 shell with Ni nanoparticles embedded in the middle surrounds a Ni yolk core. This catalyst was highly active for DRM, and it maintained activity without sintering for 90 h at 800 °C [62].

Mesoporous materials have been widely used as supports because they provide a large surface area and facile mass transfer [63, 64]. Mesoporous Al_2O_3 in particular has been widely used because it can have a strong interaction with a metal active phase, and it has high thermal stability [65, 66]. Conventional impregnation with a metal precursor might cause pore blockage. Wang et al. developed ordered mesoporous Ni-Ce-Al oxide for DRM with self-assembly induced by solvent evaporation [67]. The Ni nanoparticles were uniformly deposited in the pore channel of the mesoporous support. The catalysts showed high durability because the Ni nanoparticles did not sinter severely due to spatial confinement. It maintained high DRM activity for 80 h at 700 °C.

CO_2 hydrogenation

Reverse water-gas shift reaction

CO_2 can react with H_2 to produce CO via the reverse water gas shift reaction. The RWGS reaction was first observed in 1914 by Bosch and Wild when they tried to produce H_2 from steam and CO over FeO_x catalyst [68]. RWGS can produce syn-gas, which is useful for synthesizing valuable chemicals such as ammonia, methanol, and fuels, from CO_2 [69]. However, the RWGS reaction is endothermic, requiring high temperature, and CO is the dominant product above 600 °C as can be seen in Fig. 7 [70]. Developing catalysts with high activity and durability is essential to obtain a maximum yield.

Two reaction pathways, the redox mechanism and formate decomposition mechanism, have been reported for CO formation from RWGS. A case with a Cu catalyst followed the redox mechanism; CO_2 oxidizes Cu^0 to Cu^+ generating CO, and H_2 reduces Cu^+ to Cu^0 forming H_2O [71]. In the formate decomposition mechanism, CO_2 hydrogenates to formate, followed by cleavage of the C=O bond [72]. Catalysts for RWGS should contain active sites to dissociate hydrogen and adsorb CO_2. Precious metal-based catalysts have been widely used for RWGS because of their superior activity for hydrogen dissociation. The effect of Pt particle size on the

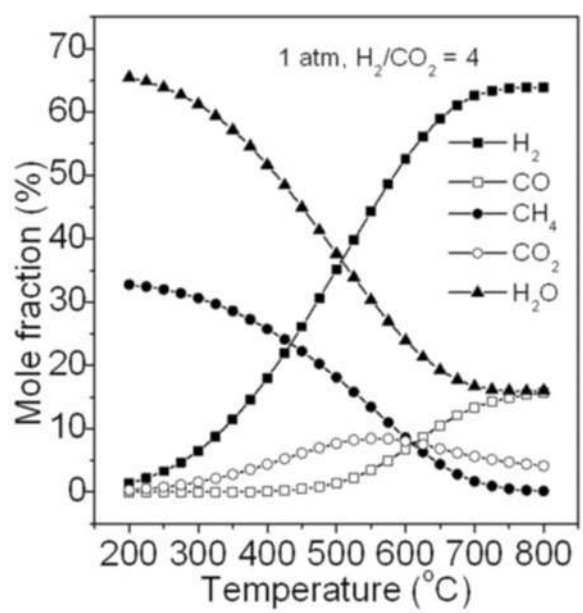

Fig. 7 Thermodynamic equilibrium of CO_2 hydrogenation at 1 bar and a H_2/CO_2 molar ratio of 4. (Reprinted with permission from [70]. Copyright 2012 Royal Society of Chemistry)

selectivity of CO and CH_4 was identified using rutile TiO_2 as a support. Small Pt particles preferred CO formation. Pt-CO species were the key intermediate deciding CO selectivity in the RWGS reaction [73].

The Au@UIO-67 catalyst was synthesized for the RWGS reaction. UIO-67, which is porous metal-organic framework, was used to disperse Au nanoparticles, then the interaction between the metal and support was enhanced. Au@UIO-67 showed high activity and CO selectivity for RWGS [74]. A Pd–In/SiO_2 catalyst was synthesized by the wet impregnation method and used for RWGS. While the Pd/SiO_2 showed 88% CO selectivity, Pd-In/SiO_2 showed 100% CO selectivity without CH_4 formation. The difference was derived from the modified CO adsorption energy. CO adsorption on the Pd-In bimetallic surface was much weaker than that on the Pd surface [75].

For the large scale conversion of CO_2, non-precious metal catalysts are preferred due to cost and scarcity. Ni and Cu-based catalysts are promising because they also show high activity and selectivity for RWGS. But they usually suffer from sintering at high reaction temperatures.

Various ways of improving thermal stability have been investigated. Rossi et al. prepared highly dispersed Ni nanoparticles supported on SiO_2 using magnetron sputtering deposition. The prepared catalyst showed better activity at T > 600 °C and stability than a conventional catalyst prepared by the wet impregnation method [76]. Ni/Ce-Zr-O catalysts were synthesized and used for RWGS. Ni species were incorporated into the lattice of a Ce-Zr-O solid solution. High activity, stability and selectivity were achieved for the conversion of CO_2 to CO [77]. Cu/ZnO catalysts with various Cu/Zn ratios were synthesized using aurichalcite precursors. The interface between the Cu and ZnO affected the catalytic activity for CO_2 activation. As the Cu ratio increased, the Cu domain size increased and the CO generation rate decreased [78]. Zheng at al. prepared CeCu composite catalysts with different Ce/Cu mole ratios for RWGS. The Ce^{3+}-oxygen vacancy-Cu^0 structure was stabilized. Cu sites became more electron deficient following electron transfer from Cu to Ce, with enhanced adsorption of CO_2 and H_2. The $Ce_{1.1}Cu_1$ catalyst showed the highest catalytic performance for the RWGS reaction [79].

Transition-metal carbides (TMCs) are promising for RWGS because they can dissociate hydrogen and C=O bonds. With their abundance and low cost, many researchers have reported on TMCs based-catalysts for RWGS. A recent study revealed that Mo_2C showed higher CO_2 conversion and CO selectivity in the RWGS than other TMCs such as TiC, TaC, ZrC, WC, and NbC [80]. The experimental and density functional theory (DFT) results showed that the oxygen binding energy and activation barriers for oxygen removal were the main factors for identifying effective catalysts for CO_2 reduction.

Willauer et al. prepared K-Mo_2C supported on γ-Al_2O_3 [81]. By modifying with a K promoter, CO selectivity and stability increased, with only 7.3% deactivation after 68 h. CO_2 adsorption was enhanced and CO_2 dissociation barriers were reduced on the K-promoted catalyst. Illas et al. reported that polycrystalline α-Mo_2C catalyst showed 16% CO_2 conversion and 99.5% CO selectivity at 673 K in RWGS [82]. The presence of a (101)-Mo/C surface on the catalyst provides active sites for RWGS. Ma et al. synthesized a highly efficient and stable Cu/β-Mo_2C catalyst for the RWGS reaction [83]. Because of strong interaction between the Cu and β-Mo_2C which dispersed the Cu particles uniformly on the support, Cu/β-Mo_2C showed high activity and stability compared with Pt- and Cu-based catalysts. Recently, Ajayan et al. reported a metal-free carbon-based catalyst for CO_2 hydrogenation [84]. Pyridinic N was doped at the edge sites of graphene quantum dots. The N dopants played a key role in inducing thermocatalytic CO_2 hydrogenation activity. CO was produced dominantly at lower temperatures and CO selectivity increased to 85% at 300 °C.

Recently, Ajayan et al. reported a metal-free carbon-based catalyst for CO_2 hydrogenation [84]. Pyridinic N was doped at the edge sites of graphene quantum dots. The N dopants played a key role in inducing thermocatalytic CO_2 hydrogenation activity. CO was produced dominantly at lower temperatures and CO selectivity increased to 85% at 300 °C.

CO_2 methanation

CO_2 hydrogenation can also produce methane. The CO_2 methanation has recently received much attention as a way to store intermittent electricity, which is produced from solar cell or wind power [85]. The surplus electricity can electrolyze water, producing H_2. Then CO_2 and the H_2 can have reaction to produce methane, which can be used as a fuel. Various precious metals, such as Ru, Rh, Pd, have been used as catalyst. Ni deposited on various supports have also been used for the CO_2 methanation [85]. Amal and Dai et al. produced methane from CO_2 and H_2 using porous perovskite materials [86, 87]. The perovskite materials with ABO_x crystalline structure have been particularly interesting materials in solar cells or catalytic applications [86]. Ni-Rh nanoalloy nanoparticles were formed by ex-solution on mesoporous $LaAlO_3$ perovskite and showed good performance for CO_2 methanation with turnover frequency of 13.9 mol/mol/h [87]. Similarly, mesoporous Ni/Co_3O_4 was

prepared with high activity for CO_2 methanation at low temperature [88].

Light-assisted CO_2 hydrogenation

Light is considered an important and ultimate energy source for CO_2 reduction, in a process also known as artificial photosynthesis. Various semiconductor-based photocatalysts have been investigated for CO_2 reduction [89, 90]. However, they typically have shown low activity and poor durability. Instead of using light for exciton production, light can be used as an auxiliary energy source to minimize overall energy usage. Recently, unique light-assisted surface reactions have been reported [91–93]. They can occur through excitation of electrons in hybridized orbitals of adsorbed reactant molecules on the metal catalyst surface.

We recently reported light-assisted CO_2 hydrogenation on heterogeneous metal catalysts [94]. Various metals were tested in a photoreactor by changing temperature, light intensity, and light wavelength. CO_2 conversion was enhanced on a Ru or Rh catalyst upon light irradiation, as shown in Fig. 8a. They produced CH_4 selectively. But Pt, Ni, Cu only produced CO without any enhancement upon light irradiation. As the light intensity increased, CO_2 conversion also increased linearly, indicating that hot electrons generated upon light irradiation were responsible for the CO_2 conversion enhancement.

In-situ UV spectroscopy results measured under CO_2 flow also confirmed that CO_2 adsorbed on the Ru surface can absorb visible light. DFT calculations showed that the band-gap energy decreased from 8.2 eV for free CO_2 to 2.4 eV for CO_2 adsorbed on Ru, as shown in Fig. 8b. This small band-gap energy enabled the absorption of visible light. The DRIFT measurement in Fig. 8c shows that CO_2 was cleaved to CO with light irradiation on a Ru catalyst. By using both light and heat, the overall energy could be reduced to 37% of the case when only heat was used, to achieve the same CO_2 conversion of 15%. Additionally, the CO_2 conversion was easily initiated or terminated simply by turning the light on or off.

Electrochemical CO_2 reduction

The electrochemical CO_2 reduction reaction (CO_2RR) involves CO_2 conversion on an electrode powered by electric bias. Because CO_2 is highly stable with a linear molecular shape having two C=O bonds, it requires a high overpotential to initiate the reaction [95]. An overpotential is the difference between the actual applied

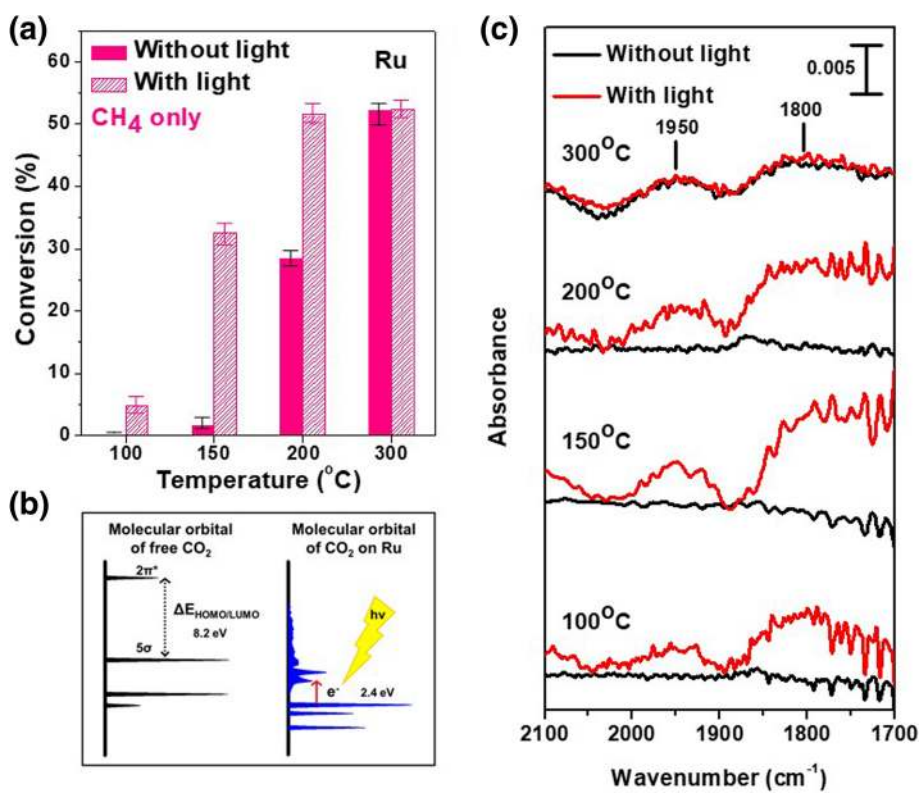

Fig. 8 a CO_2 conversion enhancement with light irradiation at various temperatures, **b** schematic diagram of hybridized orbital change and hot electron generation with light irradiation, **c** DRIFT analysis results with CO_2 flow on Ru catalysts with and without light irradiation. (Reprinted with permission from ref. [94]. Copyright 2018 Springer Nature)

potential and theoretical thermodynamic potential. Heterogeneous electrocatalysts should be used to reduce the overpotential. The performance and reaction pathway highly depend on the electrocatalyst. CO_2 is electrochemically reduced to chemicals or fuels at the cathode, and the counter anode reaction is water oxidation producing oxygen, typically known as oxygen evolution reaction (OER) [96].

A distinct feature of the electrochemical CO_2 reduction is its compatibility with renewable sources. Because CO_2 is thermodynamically stable, the CO_2 conversion involves high energy consumption [95, 97]. This energy can be obtained from renewable sources, such as solar or wind power, and the obtained electricity can drive the electrochemical CO_2RR. Additionally, electrochemical CO_2 conversion can be used for renewable energy storage [95, 98]. Since the renewable power is inherently intermittent and undistributed, storing the electricity in chemical bonds might be useful [98]. Fuels such as CH_4 can be used in current conventional power systems. Various chemicals, from several C_1 products to multi-carbon products, can be directly generated from electrochemical CO_2RR [99–101].

Various products can be obtained from the electrochemical CO_2RR. Table 1 shows several representative CO_2RR pathways with thermodynamic standard potentials versus a reversible hydrogen electrode (RHE) [96, 102]. Neutral pH buffer electrolytes have been widely used for electrochemical CO_2RR studies, and the potentials at neutral pH were shown [96]. The CO_2RR typically competes with the hydrogen evolution reaction (HER). Suppressing HER is one of the most important issues in the development of electrocatalysts for CO_2RR. In this next section, the electrocatalysts are classified according to products of CO, formate, and multi-carbon species. The metals generating each product are explained. Unconventional catalysts are additionally introduced.

Metals producing CO: Au, Ag, Zn, and Pd

Au, Ag, Zn, and Pd generate CO as a predominant product from CO_2RR [101]. CO is an important feed chemical for various chemical processes [95]. The key descriptor for CO production is the binding energy of *COOH. The metals bind to *COOH sequentially yielding *CO after dehydration, as shown in Fig. 9 [100, 103, 104]. The reaction pathway toward CO is two electron-consuming, which is relatively facile [100]. When CO is the main product, there is no separation issue because gaseous CO would be naturally separated from liquid electrolyte.

Various works controlling the nano-structures of these metals have been reported to have high CO production from CO_2RR; monodispersed Au or Ag nanoparticles [105–108], ligand-free Au nanoparticles with < 2 nm [109], inverse opal Au or Ag thin films [110, 111], ultrathin Au nanowires [112], Au nanoneedles with sharp tips [113, 114], concave rhombic dodecahedral Au nanoparticles with high-index facets [115], TiC-supported Au nanoparticles [116], hexagonal Zn particles [117], electrodeposited Zn dendrites [118], anodized Zn foil [119], small sized Pd nanoparticles with rich edge sites [120, 121], Au electrode with adsorbed CN^- or Cl^- ions [122], Ag nanoparticles with surface-bonded oxygen [123], amine-capped Ag nanoparticles [124]. Although it is hard to compare their performance because of their different reaction conditions, the conversion of CO_2 to CO usually reaches 90 ~ 100% faraday efficiency at the relatively low overpotential of 0.4 ~ 0.7 V.

Metals producing formate: Sn, Bi, Hg, Cd, and Pb

Sn, Bi, Hg, Cd, and Pb can produce formic acid (HCOOH) or formate ($HCOO^-$) in the CO_2RR [101]. The key descriptor toward formate formation is the binding energy of *OCHO [103]. If the electrode surface is bound to intermediates via oxygen rather than carbon, formic acid will be generated, as shown in Fig. 13 [103]. It was also suggested that formate could be generated through an *COOH intermediate at some reaction

Table 1 Representative reaction pathways of CO_2RR in neutral pH buffer electrolyte condition with thermodynamic standard potentials

	Reaction in neutral pH buffer electrolyte	E^0 (V vs RHE)
Cathode reaction	(CO_2RR) $CO_2 + H_2O + 2e^- \rightarrow CO + 2OH^-$	− 0.10
	(CO_2RR) $CO_2 + 2H_2O + 2e^- \rightarrow HCOOH + 2OH^-$	− 0.02
	(CO_2RR) $CO_2 + 5H_2O + 6e^- \rightarrow CH_3OH + 6OH^-$	0.03
	(CO_2RR) $CO_2 + 6H_2O + 8e^- \rightarrow CH_4 + 8OH^-$	0.17
	(CO_2RR) $2CO_2 + 8H_2O + 12e^- \rightarrow C_2H_4 + 12OH^-$	0.08
	(HER) $2H_2O + 2e^- \rightarrow H_2 + 2OH^-$	0
Anode reaction	(OER) $2H_2O \rightarrow O_2 + 4H^+ + 4e^-$	1.229

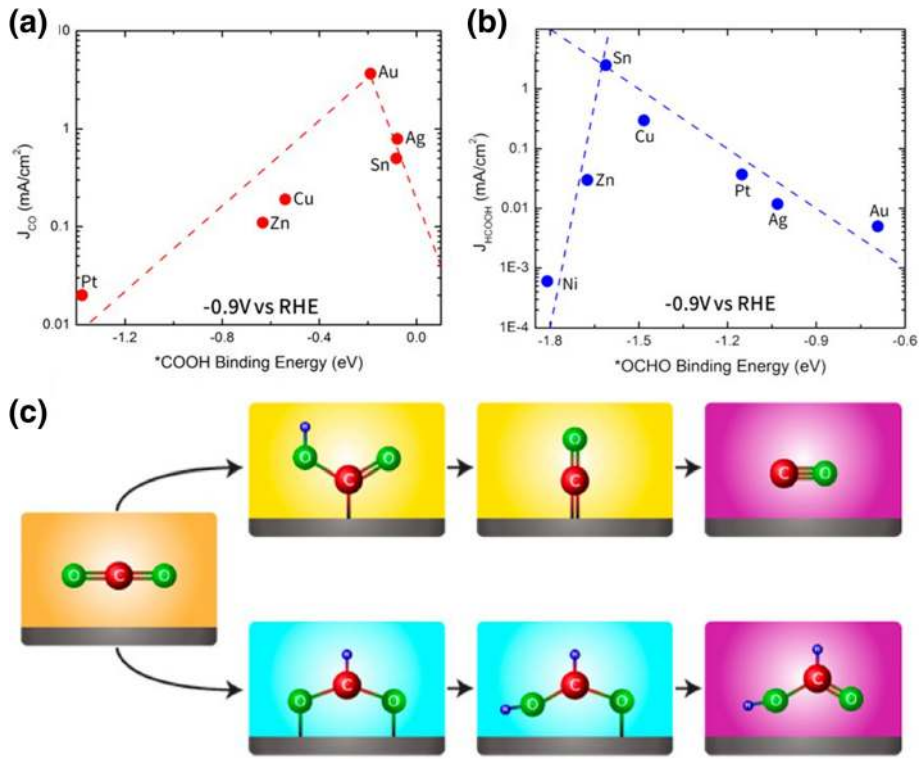

Fig. 9 Volcano plots of CO_2RR activity toward **a** CO and **b** HCOOH as a function of binding energies of *COOH, and *OCHO, respectively, and **c** CO_2RR mechanisms to CO or HCOOH. (Reprinted with permission from ref. [103]. Copyright 2017 American Chemical Society)

conditions [125, 126]. Because the pathway generating formates follows a two electron pathway, like CO, some electrocatalysts might exhibit good CO_2RR performance for formic acid production [101]. However, the faradaic efficiency for formic acid production is usually lower than that for CO production [127]. Nevertheless, formic acid is the only liquid product which can be obtained with high selectivity from CO_2RR at this stage [101].

Various studies which have controlled the nanostructures of these metals have been reported for formate production; nanostructured Sn/SnO_x thin film [128], Sn or Sn oxide nanoparticles with < 5 nm [129, 130], reduced SnO_2 porous nanowires [131], hierarchical mesoporous SnO_2 nanosheets [132], electrodeposited Sn dendrites [133], atomic layer deposited Sn or Sn sulfide on nanoneedle templates [134], ultrathin Bi nanosheets [135], oxide-derived Pb [136]. Due to toxicity of Hg, Cd, and Pb, most works have mainly used Sn or Bi. The formate can be obtained with a faraday efficiency of 60 ~ 90% at an overpotential of 0.8 ~ 1.4 V [95, 101].

On other metals, the selectivity of CO_2RR can be controlled by changing the reaction conditions to produce formic acid. For example, CO_2RR on W, Fe, Co, Ni, Zn, Pt, Rh, and Ir have been investigated at high pressure [137]. They showed significant activity toward formate formation, although their selectivity was not as high as Sn or Bi. Pd also exhibited good performance for formic acid production although it also significantly produced CO [138, 139].

Metal producing multi-carbon species: Cu

Cu is the only element that can make a C-C bond directly from CO_2RR with meaningful selectivity [95, 101]. Multi-carbon products such as C_2H_4 can be generated with Cu. Figure 10 shows the possible products obtainable from electrochemical conversion on a Cu electrode. It was reported that CO, formate, CH_4, C_2H_4, and H_2 could be obtained on a Cu electrode [140]. Ethanol, n-propanol, allyl alcohol, a trace amount of methanol, glycolaldehyde, acetaldehyde, acetate, ethylene glycol, propionaldehyde, acetone, and hydroxyacetone were simultaneously observed in the large overpotential region, higher than 1 V [140].

The reaction mechanism of CO_2RR on a Cu electrode is highly complicated. Figure 10 provides the possible reaction pathway maps. Many other pathways on the Cu electrode have also been proposed [141–143]. The *CO intermediate is generally regarded to be a key intermediate for further reduction, because *CO can be obtained at mild potentials, and C_2H_4 was observed only with significant concentrations of *CO [144–146]. The protonation of *CO to *CHO needs to overcome an activation

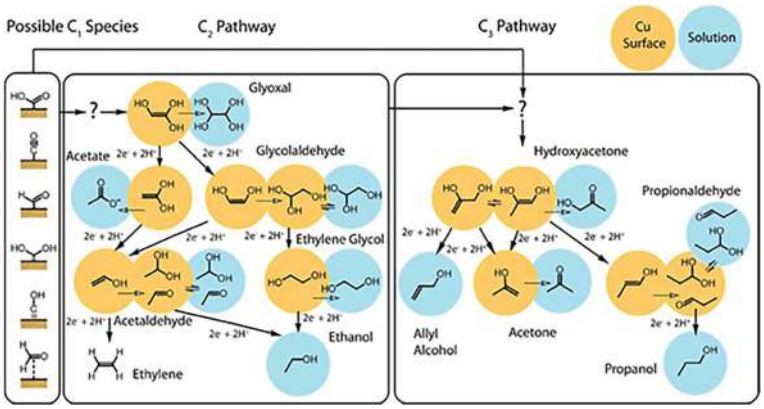

Fig. 10 Proposed reaction pathways of electrochemical CO_2RR on Cu electrode in CO_2-saturated 0.1 M $KHCO_3$(aq). (Reprinted with permission from ref. [140]. Copyright 2012 Royal Society of Chemistry)

barrier of 0.74 V, which is considered a rate-determining step for further reduction to C_1 products like CH_3OH or CH_4 [145, 147]. The *CHO transforms to *CH_2O, *CH_3O, and *CH_4 following sequential proton coupled electron transfer (PCET) [142, 147]. The *CHO is also a key intermediate for making C-C bonds via *CO-*CHO coupling [143].

Additionally, *CO-*CO coupling can also produce C-C bonds [141, 148–150]. However, the C-C coupling pathway has not been elucidated yet, although it is known that Cu (100) is the best surface to generate *CO-*CO coupling with the lowest energy barrier [150, 151]. As a result, C_2H_4 formation is favored on Cu (100) [151–153], whereas CH_4 is more readily produced on Cu (111) [147, 154]. The pathways for further reduction from *CO-*CO or *CHO-*CO to oxygenates, such as acetate, ethanol, 1-propanol, are more complicated, because water from the electrolyte participates in the reaction donating oxygen [143, 148]. Because it is crucial to understand the reaction mechanism to design better catalysts for CO_2RR, more studies on mechanism or intermediates, such as in-situ experiments, are needed.

To tune selectivity, nano-structured Cu electrodes were studied, including Cu nanofoams [155], Cu nanowires [156–160], nanoporous Cu film [161], Cu nanocubes [151–153], Cu truncated nanocubes [153], Cu rhombic dodecahedrons [153], inverse opal Cu film [162], mesoporous Cu film [163], electro-redeposited Cu [164], electrodeposited Cu dendrites [165], prism shaped Cu [166], nano-structured Cu by battery cycling [150], hierarchical Cu pillar electrode [167], oxide derived Cu [160, 168–170]. The best CO_2RR performance on Cu electrode was 60 ~ 70% faraday efficiency toward C_2H_4 production [170, 171].

Unconventional electrocatalysts

So far, electrochemical CO_2RR with single metal electrodes has been discussed. The studies with single metal electrodes can provide insight in terms of reaction mechanisms and the properties of each metal on CO_2RR. Some unconventional electrocatalysts, such as oxide-derived metals, alloy metals, carbon materials, single-atom catalyst, have also exhibited interesting features. Distinct selectivity or activity was obtained.

Oxide-derived metals

Recent studies have revealed that oxide-derived metal electrodes had improved catalytic performance compared to pristine metals [172]. The most common way to prepare oxide-derived electrocatalysts is to oxidize the metal, then reduce it to its original metallic state. Oxide-derived Cu produced more C_2 products of C_2H_4, C_2H_6, and ethanol than electro-polished Cu at the same overpotential [168, 170, 172]. Even C_3 and C_4 products of C_3H_7OH, C_3H_6, C_3H_8, C_4H_{10} were observed from Cl ion-adsorbed oxide-derived Cu [173]. Oxide-derived Sn showed much higher current density and faraday efficiency than a pristine Sn electrode for formic acid production [128, 133]. Oxide-derived Au [174] or Ag [175] showed superior faraday efficiency for CO production, with 90 ~ 100% at only 0.3 V overpotential, as shown in Fig. 11a.

There have been debates on the origin of the enhancement of oxide-derived metal for CO_2RR. Nano-structures induced in the catalysts or residual subsurface oxygen have been suggested as the source of the enhancement. Nano-structured surfaces with rich grain boundaries were obtained after oxidation-reduction cycling [176, 177]. The induced surface had more defect sites with higher binding energy to *CO and higher local pH which increased

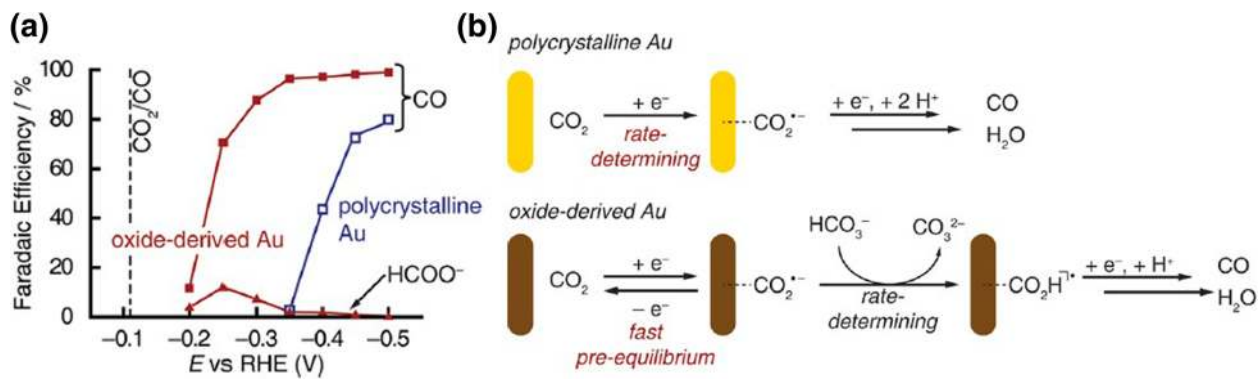

Fig. 11 Electrocatalytic CO_2RR on oxide-derived Au and polycrystalline Au. **a** Faraday efficiency of each product as a function of applied potential and **b** proposed reaction mechanisms. (Reprinted with permission from ref. [174]. Copyright 2012 American Chemical Society)

selectivity toward CO_2RR while suppressing HER [169, 176–178]. It was also suggested that some oxygen remained in the subsurface despite the highly reducing conditions of the CO_2RR. Ambient pressure XPS, in situ electron energy loss spectroscopy (EELS) experiments, and DFT calculations showed that the oxygen helped to activate CO_2 on the surface in the initial step, as shown in Fig. 11b [179, 180]. However, a contradictory result was also reported, saying that the residual oxide was very unstable in the CO_2RR condition, and that the amount of oxygen was negligible [181].

Alloy metals

By alloying with a secondary metal, the intrinsic catalytic performance of metal can be modified, and high selectivity or activity can be obtained for CO_2RR [101, 127]. The enhancement was typically attributed to an electronic or geometric effect on the alloyed catalysts [101, 127]. The presence of a secondary metal led to modulation in the electronic structure of the active site. The binding energy between the active site and reaction intermediate could be tuned, changing the reaction pathway and the resulting selectivity [182–185]. The secondary metal can also change the surface geometric structure, with different atomic arrangements of reactant or intermediates. The electronic and geometric effect has been systematically studied for Au-Cu bimetallic nanoparticle catalysts with different compositions [183, 184]. Figure 12a shows that the *d*-band center was downshifted as Au content increased, and the change in the electronic structure lowered the binding energy of *COOH and *CO. The Cu atom was bound to the oxygen end of the *COOH, while the Au atom formed a Au-C bond [183]. The binding strength of each primary bond and the adsorption configuration were tailored by changing the composition of the bimetallic particles. The ordered Au-Cu with three atomic overlayers of Au showed high performance for CO production due to the change in binding energy induced by atomic strains [184]. The reaction path to the C-C coupling was suppressed by the geometric property of the ordered Au_3Cu alloys, producing CH_4 [185].

The alloy catalysts deviate from the general scaling relationship of binding strength to intermediates, and by controlling mixing patterns, they can exhibit unique selectivity. For example, while ordered Cu-Pd nanoparticles selectively produced C_1 products, mainly CO, but phase-separated Cu-Pd nanoparticles produced C_2 products, mainly C_2H_4 [185]. Cu ensemble sites were needed to make C-C bonds, and neighboring Pd sites further helped hydrogenation by hydrogen spillover.

For multi-electron paths rather than a two-electron path, the key intermediates of *CHO or *COH should be formed, but proton-coupled electron transfer on *CO to form *CHO or *COH is a rate determining step [101]. It was reported that if Cu was alloyed with a metal that could stabilize O, the adsorption configuration of *CHO or *COH on the Cu-M sites could be adjusted and their formation would be favored [186]. Consequently, the overpotential for further reduction decreased and the selectivity of CO_2RR could be controlled. Many other alloy catalysts were reported for CO_2RR; Cu-In [187], Cu-Sn [188] for CO production, Pd-Pt [189], Ag-Sn [190], Sn-Pb [191], Sn-Pd [192], Au-Pd [193] for formate production.

Carbon-based materials

Carbon-based materials have been actively studied as promising electrocatalysts for electrochemical reactions, such as the oxygen reduction reaction (ORR), OER, and HER [194, 195]. Carbon materials have advantages for electrochemical applications, including facile transformability to various dimensions and shapes [196]. Zero-dimensional carbon dots or graphene quantum dots, one-dimensional carbon nanotubes, two-dimensional

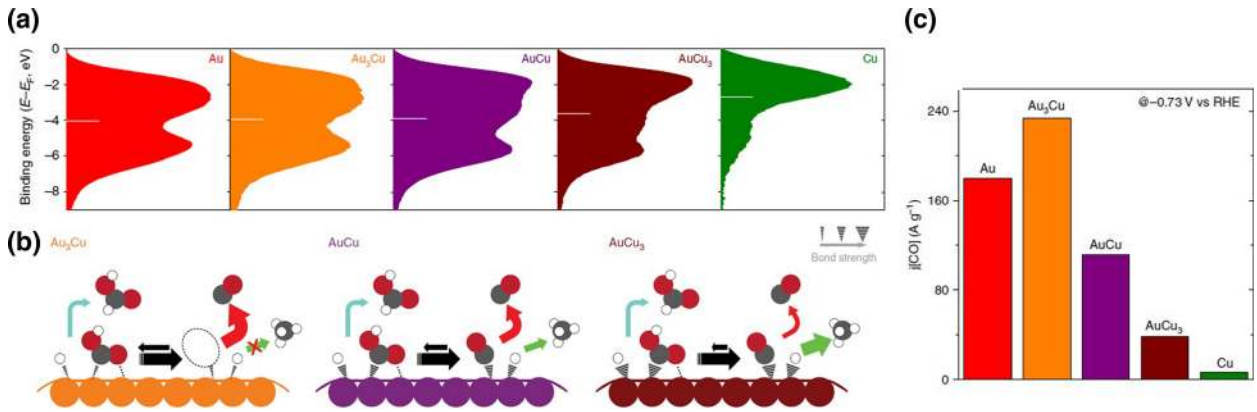

Fig.12 Tailored properties of Au-Cu alloy nanoparticle catalyst for CO_2RR with different compositions. **a** Electronic structure information obtained with high-resolution X-ray photoemission spectroscopy (XPS), **b** scheme for the reaction mechanism on the surface of alloy catalysts, and **c** overall mass activity to CO production at − 0.73 V_{RHE}. (Reprinted with permission from ref. [183]. Copyright 2014 Springer Nature)

graphene, and three-dimensional graphene aerogel can be produced with well-developed material science techniques [97]. The carbon materials also possess high conductivity, high surface area, and good chemical and mechanical stability.

Pure carbon materials are basically inert toward CO_2RR. However, if heteroatoms such as N are doped in the carbon matrix, electrocatalytic activity is greatly enhanced. Negatively charged N sites are considered active sites for CO_2RR [197–199]. N-doping introduces a Lewis base site to the catalyst, which is beneficial to stabilize CO_2 [196, 197]. Various carbon materials, including N-doped carbon nanotubes [200, 201], N-doped graphenes [202], N-doped graphene quantum dots [203] were reported for CO_2RR following the two-electron pathway. N-doped diamond produced acetate as well as formate with N-sp^3C active sites [204]. Other dopants such as S or B have also been used for CO_2RR [205, 206].

Single atom catalysts

Single atom catalysts (SAC) represent atomically dispersed metal catalysts on the surface of a support. They exhibit very distinct electronic structures and adsorption configurations of reactants and intermediates, with unique selectivity [207]. SACs have been used for electrochemical ORR [208, 209], HER [210], formic acid oxidation reaction (FAOR) [211], and CO_2RR [212]. Ni single atoms on N-doped graphene can catalyze CO_2RR producing CO selectively, as shown in Fig. 13 [212]. Other metal atoms of Fe, Co, Mn, and Cu with slightly different *d*-band structure have shown different selectivity. The coordination environment neighboring the Ni single atom has also been reported to affect the electronic structure and the binding energy of key carbon intermediates [213, 214]. When Cu was atomically doped into CeO_2, the oxygen defect sites of the CeO_2 regulated the oxidation state of Cu by forming Cu ion-O vacancy pairs. The single atomic Cu catalyzed CO_2RR, producing CH_4 with 58% faraday efficiency [215]. DFT calculations have also predicted that the SAC structure can suppress HER while promoting CO_2RR, with the proper choice of metal atom and supports [216, 217]. Single atom alloys where a single atomic metal is located on another metal surface have also been suggested by computational method as efficient catalysts for CO_2RR [218].

Although many intensive efforts have been dedicated to develop electrochemical CO_2RR, the performance is still far from the performance obtained from gas-phase CO_2 reduction. To enhance electrochemical CO_2RR further, various other efforts have been tried, by tuning other factors. Electrolyte compositions, pH, and concentrations affected activity and selectivity [96, 219–222]. Ionic liquids helped the activation of CO_2 [223, 224]. An electric field near the electrode was shown to stabilize charged intermediates better [113, 220]. The additives could control selectivity via electron shuttling or the formation of surface films [225, 226]. A gas diffusion electrode (GDE) cell allowed unprecedentedly high current density [171, 227]. Stability, resistivity to catalyst poisons, and activity on diluted CO_2 feed are also important for practical applications, but they have not yet attracted much interest at this stage. To develop this technology to a commercially feasible level, those many factors should be optimized.

Conclusion and perspectives

Heterogeneous catalysts used for catalytic CO_2 conversion into valuable chemicals such as CO, CH_4, C_2H_4 have been discussed in this review. Because CO_2 is thermodynamically very stable, its conversion usually

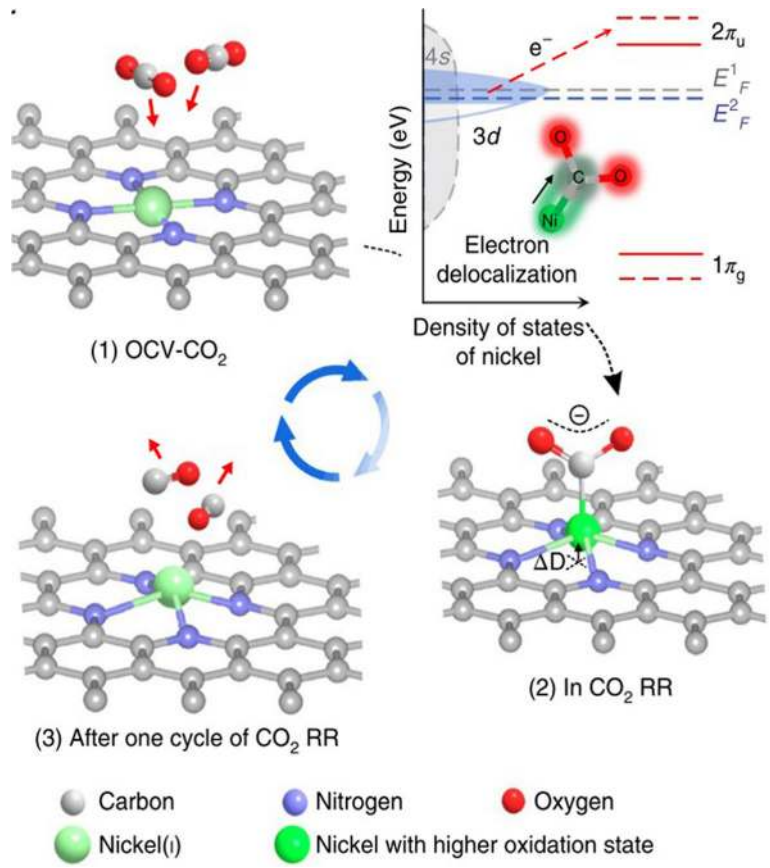

Fig. 13 Structural evolution of Ni single-atom sites on graphene during CO_2RR (Reprinted with permission from ref. [212]. Copyright 2018 Springer Nature)

requires a lot of energy, but the production of that energy also emits considerable CO_2. Obtaining negative net CO_2 emissions is not easy, and the design of efficient catalysts for CO_2 conversion is a key to reducing CO_2 emissions.

Catalytic CO_2 conversion can occur in gas-phase, liquid-phase, or electrochemical cells. Because the solubility of CO_2 is quite low in aqueous solution, the CO_2 conversion in liquid-phase typically suffer from low productivity. Thus this review mainly focused on the conversion using gaseous CO_2. Various metals, metal oxides, metal carbides, and doped carbon materials have been used as catalysts for CO_2 conversion. Synthetic strategies have been developed to endure high reaction temperatures and minimize coke formation for dry methane reforming. The CO_2 hydrogenation can be efficient, but they use H_2 gas. The H_2 gas is conventionally produced from methane steam reforming, which also produces considerable CO_2. If H_2 can be produced from water without CO_2 emissions, CO_2 hydrogenation in gas-phase would be a very powerful tool for efficient CO_2 conversion. The gaseous product of CO or CH_4 have been mainly considered as products from the CO_2 hydrogenation, but liquid products such as formic acid or dimethyl ether would also have high value. Metal-based catalysts including precious metal or supported Ni catalysts have been used for the production of CO or CH_4. Not many good heterogeneous catalysts have been found for the production of formic acid, instead homogeneous catalysts have been typically used. Robust heterogeneous catalyst producing formic acid might have high potential. Catalysts that use both heat and light as energy sources have been developed, to minimize total energy use.

Electrochemical CO_2 conversion has shown improved productivity using gas-diffusion electrode cells. It is also very promising because it directly uses CO_2 and H_2O for chemical or fuel production. The technology for electrochemical CO_2 reduction is in its early stages, compared to other CO_2 conversion technologies, but it is being investigated very actively. A variety of materials have been tested as catalysts for electrochemical CO_2 reduction, and the catalysts should be tuned depending on the target products. Au or Ag produces CO, Sn or Bi produces formate, and Cu produces hydrocarbons such as C_2H_4. Considering the cell design of gas-diffusion electrodes, nano-structured catalysts should be optimized further. Most studies so far have used concentrated pure CO_2

for the conversion. But the conversion of dilute CO_2, especially in the presence of potential catalyst poisons such as S compounds, should be investigated more actively for practical applications.

Abbreviations
CO2RR: Electrochemical CO_2 reduction reaction; DFT: Density functional theory; DRM: Dry reforming of methane; EELS: Electron energy loss spectroscopy; EXAFS: Extended X-ray absorption fine structure; GDE: Gas diffusion electrode; HER: Hydrogen evolution reaction; OER: Oxygen evolution reaction; ORR: Oxygen reduction reaction; POM: Partial oxidation of methane; RHE: Reversible hydrogen electrode; RWGS: Reverse water gas shift; SAC: Single atom catalysts; SMSI: Strong-metal support interaction; SRM: Steam reforming of methane; TMC: Transition-metal carbide; XAFS: X-ray absorption fine structure; XANES: X-ray absorption near edge structure

Acknowledgements
Not applicable

Funding
This work was financially supported by the National Research Foundation of Korea (NRF-2017M3D1A1040692) funded by the Ministry of Education, Science and Technology and the Saudi Aramco-KAIST CO_2 Management Center.

Availability of data and materials
Not applicable

Authors' contributions
HL organized the overall structure. HSW wrote the manuscript about DRM, MSC wrote the manuscript about RWGS, JLee wrote the manuscript about light-assisted CO_2 hydrogenation, JLim wrote the manuscript about CO_2RR. All authors read and approved the final manuscript.

Competing interests
The authors declare that they have no competing interests.

Publisher's Note
Springer Nature remains neutral with regard to jurisdictional claims in published maps and institutional affiliations.

Received: 1 November 2018 Accepted: 22 February 2019
Published online: 27 March 2019

References
1. Hansen J, Ruedy R, Sato M, Lo K. Global surface temperature change. Rev Geophys. 2010;48:RG4004.
2. Dincer I. Renewable energy and sustainable development: a crucial review. Renew Sust Energ Rev. 2000;4(2):157–75.
3. Burke MJ, Stephens JC. Political power and renewable energy futures: a critical review. Energy Res Soc Sci. 2018;35:78–93.
4. Alvarez A, Bansode A, Urakawa A, Bavykina AV, Wezendonk TA, Makkee M, Gascon J, Kapteijn F. Challenges in the greener production of formates/formic acid, methanol, and DME by heterogeneously catalyzed CO_2 hydrogenation processes. Chem Rev. 2017;117(14):9804–38.
5. Lim RJ, Xie M, Sk MA, Lee J-M, Fisher A, Wang X, Lim KH. A review on the electrochemical reduction of CO_2 in fuel cells, metal electrodes and molecular catalysts. Catal Today. 2014;233:169–80.
6. Porosoff MD, Yan B, Chen JG. Catalytic reduction of CO_2 by H_2 for synthesis of CO, methanol and hydrocarbons: challenges and opportunities. Energy Environ Sci. 2016;9(1):62–73.
7. Yan N, Philippot K. Transformation of CO_2 by using nanoscale metal catalysts: cases studies on the formation of formic acid and dimethylether. Curr Opin Chem Eng. 2018;20:86–92.
8. Wang WH, Himeda Y, Muckerman JT, Manbeck GF, Fujita E. CO_2 hydrogenation to formate and methanol as an alternative to photo- and electrochemical CO_2 reduction. Chem Rev. 2015;115(23):12936–73.
9. Li WH, Wang HZ, Jiang X, Zhu J, Liu ZM, Guo XW, Song CS. A short review of recent advances in CO_2 hydrogenation to hydrocarbons over heterogeneous catalysts. RSC Adv. 2018;8(14):7651–69.
10. Li K, Peng BS, Peng TY. Recent advances in heterogeneous photocatalytic CO_2 conversion to solar fuels. ACS Catal. 2016;6(11):7485–527.
11. Gunasekar GH, Park K, Jung KD, Yoon S. Recent developments in the catalytic hydrogenation of CO_2 to formic acid/formate using heterogeneous catalysts. Inorg Chem Front. 2016;3(7):882–95.
12. Kawi S, Kathiraser Y, Ni J, Oemar U, Li ZW, Saw ET. Progress in synthesis of highly active and stable nickel-based catalysts for carbon dioxide reforming of methane. ChemSusChem. 2015;8(21):3556–75.
13. Pakhare D, Spivey J. A review of dry (CO_2) reforming of methane over noble metal catalysts. Chem Soc Rev. 2014;43(22):7813–37.
14. York APE, Xiao TC, Green MLH. Brief overview of the partial oxidation of methane to synthesis gas. Top Catal. 2003;22(3–4):345–58.
15. Kim HY, Park JN, Henkelman G, Kim JM. Design of a highly nanodispersed Pd-MgO/SiO_2 composite catalyst with multifunctional activity for CH_4 reforming. ChemSusChem. 2012;5(8):1474–81.
16. Gallego GS, Batiot-Dupeyrat C, Barrault J, Florez E, Mondragon F. Dry reforming of methane over $LaNi_{1-y}B_yO^{3+/-delta}$(B=Mg, Co) perovskites used as catalyst precursor. Appl Catal A. 2008;334(1–2):251–8.
17. Pakhare D, Shaw C, Haynes D, Shekhawat D, Spivey J. Effect of reaction temperature on activity of Pt- and Ru-substituted lanthanum zirconate pyrochlores ($La_2Zr_2O_7$) for dry (CO_2) reforming of methane (DRM). J CO2 Util. 2013;1:37–42.
18. Bian ZF, Das S, Wai MH, Hongmanorom P, Kawi S. A review on bimetallic nickel-based catalysts for CO_2 reforming of methane. ChemPhysChem. 2017;18(22):3117–34.
19. Arora S, Prasad R. An overview on dry reforming of methane: strategies to reduce carbonaceous deactivation of catalysts. RSC Adv. 2016;6(110):108668–88.
20. Aramouni NAK, Touma JG, Abu Tarboush B, Zeaiter J, Ahmad MN. Catalyst design for dry reforming of methane: analysis review. Renew Sust Energ Rev. 2018;82:2570–85.
21. Wang SB, Lu GQM, Millar GJ. Carbon dioxide reforming of methane to produce synthesis gas over metal-supported catalysts: state of the art. Energy Fuel. 1996;10(4):896–904.
22. Kambolis A, Matralis H, Trovarelli A, Papadopoulou C. Ni/CeO_2-ZrO_2 catalysts for the dry reforming of methane. Appl Catal A. 2010;377(1–2):16–26.
23. Sutthiumporn K, Maneerung T, Kathiraser Y, Kawi S. CO_2 dry-reforming of methane over $La_{0.8}Sr_{0.2}Ni_{0.8}M_{0.2}O_3$ perovskite (M = Bi, Co, Cr, Cu, Fe): roles of lattice oxygen on C-H activation and carbon suppression. Int J Hydrog Energy. 2012;37(15):11195–207.
24. Bhavani AG, Kim WY, Lee JS. Barium substituted lanthanum manganite perovskite for CO_2 reforming of methane. ACS Catal. 2013;3(7):1537–44.
25. Hu YH. Solid-solution catalysts for CO_2 reforming of methane. Catal Today. 2009;148(3–4):206–11.
26. Zanganeh R, Rezaei M, Zamaniyan A. Dry reforming of methane to synthesis gas on NiO-MgO nanocrystalline solid solution catalysts. Int J Hydrog Energy. 2013;38(7):3012–8.
27. Garcia-Dieguez M, Pieta IS, Herrera MC, Larrubia MA, Malpartida I, Alemany LJ. Transient study of the dry reforming of methane over Pt supported on different gamma-Al_2O_3. Catal Today. 2010;149(3–4):380–7.
28. Yokota S, Okumura K, Niwa M. Support effect of metal oxide on Rh catalysts in the CH_4-CO_2 reforming reaction. Catal Lett. 2002;84(1–2):131–4.
29. Menad S, Ferreira-Aparicio P, Cherifi O, Guerrero-Ruiz A, Rodriguez-Ramos I. Designing new high oxygen mobility supports to improve the stability of RU catalysts under dry reforming of methane. Catal Lett. 2003;89(1–2):63–7.
30. Ferreira-Aparicio P, Guerrero-Ruiz A, Rodriguez-Ramos I. Comparative study at low and medium reaction temperatures of syngas production by methane reforming with carbon dioxide over silica and alumina supported catalysts. Appl Catal A. 1998;170(1):177–87.
31. Whang HS, Choi MS, Lim J, Kim C, Heo I, Chang TS, Lee H. Enhanced activity and durability of Ru catalyst dispersed on zirconia for dry reforming of methane. Catal Today. 2017;293:122–8.
32. Park J-H, Yeo S, HeO I, Chang T-S. Promotional effect of Al addition on the Co/ZrO_2 catalyst for dry reforming of CH_4. Appl Catal A. 2018;562:120.
33. Park J-H, Yeo S, Kang T-J, Heo I, Lee K-Y, Chang T-S. Enhanced stability of co catalysts supported on phosphorus-modified Al_2O_3 for dry reforming of CH_4. Fuel. 2018;212:77–87.
34. Ay H, Uner D. Dry reforming of methane over CeO_2 supported Ni, Co and Ni-Co catalysts. Appl Catal B. 2015;179:128–38.
35. Miura H, Endo K, Ogawa R, Shishido T. Supported palladium-gold alloy catalysts for efficient and selective hydrosilylation under mild conditions

with isolated single palladium atoms in alloy nanoparticles as the main active site. ACS Catal. 2017;7(3):1543–53.
36. Kim SM, Abdala PM, Margossian T, Hosseini D, Foppa L, Armutlulu A, van Beek W, Comas-Vives A, Coperet C, Muller C. Cooperativity and dynamics increase the performance of NiFe dry reforming catalysts. J Am Chem Soc. 2017;139(5):1937–49.
37. Nakamura J, Aikawa K, Sato K, Uchijima T. Role of support in reforming of CH_4 with CO_2 over Rh catalysts. Catal Lett. 1994;25(3–4):265–70.
38. Liu DP, Quek XY, Cheo WNE, Lau R, Borgna A, Yang YH. MCM-41 supported nickel-based bimetallic catalysts with superior stability during carbon dioxide reforming of methane: effect of strong metal-support interaction. J Catal. 2009;266(2):380–90.
39. Guo JJ, Lou H, Zhao H, Chai DF, Zheng XM. Dry reforming of methane over nickel catalysts supported on magnesium aluminate spinels. Appl Catal A. 2004;273(1–2):75–82.
40. Ferreira-Aparicio P, Rodriguez-Ramos I, Anderson JA, Guerrero-Ruiz A. Mechanistic aspects of the dry reforming of methane over ruthenium catalysts. Appl Catal A. 2000;202(2):183–96.
41. Zhang ZL, Verykios XE, MacDonald SM, Affrossman S. Comparative study of carbon dioxide reforming of methane to synthesis gas over Ni/La_2O_3 and conventional nickel-based catalysts. J Phys Chem. 1996;100(2):744–54.
42. Alipour Z, Rezaei M, Meshkani F. Effect of alkaline earth promoters (MgO, CaO, and BaO) on the activity and coke formation of Ni catalysts supported on nanocrystalline Al_2O_3 in dry reforming of methane. Ind Eng Chem Res. 2014;20(5):2858–63.
43. Bellido JDA, De Souza JE, M'Peko JC, Assaf EM. Effect of adding CaO to ZrO_2 support on nickel catalyst activity in dry reforming of methane. Appl Catal A. 2009;358(2):215–23.
44. Pechimuthu NA, Pant KK, Dhingra SC, Bhalla R. Characterization and activity of K, CeO_2, and Mn promoted Ni/Al_2O_3 catalysts for carbon dioxide reforming of methane. Ind Eng Chem Res. 2006;45(22):7435–43.
45. Therdthianwong S, Therdthianwong A, SiangChin C, Yonprapat S. Synthesis gas production from dry reforming of methane over Ni/Al_2O_3 stabilized by ZrO_2. Int J Hydrog Energy. 2008;33(3):991–9.
46. Laosiripojana N, Sutthisripok W, Assabumrungrat S. Synthesis gas production from dry reforming of methane over CeO_2 doped Ni/Al_2O_3: influence of the doping ceria on the resistance toward carbon formation. Chem Eng J. 2005; 112(1–3):13–22.
47. Liang TY, Lin CY, Chou FC, Wang MQ, Tsai DH. Gas-phase synthesis of Ni-CeO_x hybrid nanoparticles and their synergistic catalysis for simultaneous reforming of methane and carbon dioxide to syngas. J Phys Chem C. 2018; 122(22):11789–98.
48. Bellido JDA, Assaf EM. Effect of the Y_2O_3-ZrO_2 support composition on nickel catalyst evaluated in dry reforming of methane. Appl Catal A. 2009; 352(1–2):179–87.
49. Wang N, Chu W, Zhang T, Zhao XS. Synthesis, characterization and catalytic performances of Ce-SBA-15 supported nickel catalysts for methane dry reforming to hydrogen and syngas. Int J Hydrog Energy. 2012;37(1):19–30.
50. Damyanova S, Pawelec B, Arishtirova K, Huerta MVM, Fierro JLG. The effect of CeO_2 on the surface and catalytic properties of Pt/CeO_2-ZrO_2 catalysts for methane dry reforming. Appl Catal B. 2009;89(1–2):149–59.
51. Zhu YA, Chen D, Zhou XG, Yuan WK. DFT studies of dry reforming of methane on Ni catalyst. Catal Today. 2009;148(3–4):260–7.
52. Ni J, Chen LW, Lin JY, Kawi S. Carbon deposition on borated alumina supported nano-sized Ni catalysts for dry reforming of CH_4. Nano Energy. 2012;1(5):674–86.
53. Han JW, Kim C, Park JS, Lee H. Highly coke-resistant Ni nanoparticle catalysts with minimal sintering in dry reforming of methane. ChemSusChem. 2014;7(2):451–6.
54. Lu JL, Fu BS, Kung MC, Xiao GM, Elam JW, Kung HH, Stair PC. Coking- and sintering-resistant palladium catalysts achieved through atomic layer deposition. Science. 2012;335(6073):1205–8.
55. Han JW, Park JS, Choi MS, Lee H. Uncoupling the size and support effects of Ni catalysts for dry reforming of methane. Appl Catal B. 2017;203:625–32.
56. Gould TD, Izar A, Weimer AW, Falconer JL, Medlin JW. Stabilizing Ni catalysts by molecular layer deposition for harsh, dry reforming conditions. ACS Catal. 2014;4(8):2714–7.
57. Das S, Ashok J, Bian Z, Dewangan N, Wai MH, Du Y, Borgna A, Hidajat K, Kawi S. Silica-ceria sandwiched Ni core-shell catalyst for low temperature dry reforming of biogas: coke resistance and mechanistic insights. Appl Catal B. 2018;230:220–36.
58. Song H. Metal hybrid nanoparticles for catalytic organic and photochemical transformations. Acc Chem Res. 2015;48(3):491–9.
59. Chaudhuri RG, Paria S. Core/shell nanoparticles: classes, properties, synthesis mechanisms, characterization, and applications. Chem Rev. 2012;112(4):2373–433.
60. Cargnello M, Jaen JJD, Garrido JCH, Bakhmutsky K, Montini T, Gamez JJC, Gorte RJ, Fornasiero P. Exceptional activity for methane combustion over modular Pd@CeO_2 subunits on functionalized Al_2O_3. Science. 2012; 337(6095):713–7.
61. Joo SH, Park JY, Tsung CK, Yamada Y, Yang PD, Somorjai GA. Thermally stable Pt/mesoporous silica core-shell nanocatalysts for high-temperature reactions. Nat Mater. 2009;8(2):126–31.
62. Li ZW, Mo LY, Kathiraser Y, Kawi S. Yolk-satellite-shell structured Ni-Yolk@Ni@SiO_2 nanocomposite: superb catalyst toward methane CO_2 reforming reaction. ACS Catal. 2014;4(5):1526–36.
63. Wang K, Li XJ, Ji SF, Shi XJ, Tang JJ. Effect of $Ce_xZr_{1-x}O_2$ promoter on Ni-based SBA-15 catalyst for steam reforming of methane. Energy Fuel. 2009;23(1–2):25–31.
64. Joo SH, Choi SJ, Oh I, Kwak J, Liu Z, Terasaki O, Ryoo R. Ordered nanoporous arrays of carbon supporting high dispersions of platinum nanoparticles. Nature. 2001;412(6843):169–72.
65. Wu Z, Li Q, Feng D, Webley PA, Zhao D. Ordered mesoporous crystalline γ-Al_2O_3 with variable architecture and porosity from a single hard template. J Am Chem Soc. 2010;132(34):12042–50.
66. Yuan Q, Yin A-X, Luo C, Sun L-D, Zhang Y-W, Duan W-T, Liu H-C, Yan C-H. Facile synthesis for ordered mesoporous γ-aluminas with high thermal stability. J Am Chem Soc. 2008;130(11):3465–72.
67. Wang N, Shen K, Huang LH, Yu XP, Qian WZ, Chu W. Facile route for synthesizing ordered mesoporous Ni-Ce-Al oxide materials and their catalytic performance for methane dry reforming to hydrogen and syngas. ACS Catal. 2013;3(7):1638–51.
68. Bosch C, Wild W. Producing hydrogen. In: Google patents; 1914.
69. Fang KG, Li DB, Lin MG, Xiang ML, Wei W, Sun YH. A short review of heterogeneous catalytic process for mixed alcohols synthesis via syngas. Catal Today. 2009;147(2):133–8.
70. Gao JJ, Wang YL, Ping Y, Hu DC, Xu GW, Gu FN, Su FB. A thermodynamic analysis of methanation reactions of carbon oxides for the production of synthetic natural gas. RSC Adv. 2012;2(6):2358–68.
71. Gines MJL, Marchi AJ, Apesteguia CR. Kinetic study of the reverse water-gas shift reaction over CuO/ZnO/Al_2O_3 catalysts. Appl Catal A. 1997;154(1–2):155–71.
72. Chen CS, Cheng WH, Lin SS. Mechanism of CO formation in reverse water-gas shift reaction over Cu/Al_2O_3 catalyst. Catal Lett. 2000;68(1–2):45–8.
73. Chen XD, Su X, Duan HM, Liang BL, Huang YQ, Zhang T. Catalytic performance of the Pt/TiO_2 catalysts in reverse water gas shift reaction: controlled product selectivity and a mechanism study. Catal Today. 2017;281:312–8.
74. Xu HT, Li YS, Luo XK, Xu ZL, Ge JP. Monodispersed gold nanoparticles supported on a zirconium-based porous metal-organic framework and their high catalytic ability for the reverse water-gas shift reaction. Chem Commun. 2017;53(56):7953–6.
75. Ye J, Ge Q, Liu CJ. Effect of PdIn bimetallic particle formation on CO_2 reduction over the Pd-In/SiO_2 catalyst. Chem Eng Sci. 2015;135:193–201.
76. Goncalves RV, Vono LLR, Wojcieszak R, Dias CSB, Wender H, Teixeira-Neto E, Rossi LM. Selective hydrogenation of CO_2 into CO on a highly dispersed nickel catalyst obtained by magnetron sputtering deposition: a step towards liquid fuels. Appl Catal B. 2017;209:240–6.
77. Sun FM, Yan CF, Wang ZD, Guo CQ, Huang SL. Ni/Ce-Zr-O catalyst for high CO_2 conversion during reverse water gas shift reaction (RWGS). Int J Hydrog Energy. 2015;40(46):15985–93.
78. Galvan CA, Schumann J, Behrens M, Fierro JLG, Schlogl R, Frei E. Reverse water-gas shift reaction at the Cu/ZnO interface: influence of the Cu/Zn ratio on structure-activity correlations. Appl Catal B. 2016;195:104–11.
79. Zhou GL, Dai BC, Xie HM, Zhang GZ, Xiong K, Zheng XX. CeCu composite catalyst for CO synthesis by reverse water-gas shift reaction: effect of Ce/Cu mole ratio. J CO2 UTIL. 2017;21:292–301.
80. Porosoff MD, Kattel S, Li WH, Liu P, Chen JG. Identifying trends and descriptors for selective CO_2 conversion to CO over transition metal carbides. Chem Commun. 2015;51(32):6988–91.
81. Porosoff MD, Baldwin JW, Peng X, Mpourmpakis G, Willauer HD. Potassium-promoted molybdenum carbide as a highly active and selective catalyst for CO_2 conversion to CO. ChemSusChem. 2017;10(11):2408–15.
82. Liu XY, Kunkel C, de la Piscina PR, Homs N, Vines F, Illas F. Effective and highly selective CO generation from CO_2 using a polycrystalline alpha-Mo_2C catalyst. ACS Catal. 2017;7(7):4323–35.

83. Zhang X, Zhu XB, Lin LL, Yao SY, Zhang MT, Liu X, Wang XP, Li YW, Shi C, Ma D. Highly dispersed copper over beta-Mo_2C as an efficient and stable catalyst for the reverse water gas shift (RWGS) reaction. ACS Catal. 2017;7(1):912–8.
84. Wu JJ, Wen C, Zou XL, Jimenez J, Sun J, Xia YJ, Rodrigues MTF, Vinod S, Zhong J, Chopra N, et al. Carbon dioxide hydrogenation over a metal-free carbon-based catalyst. ACS Catal. 2017;7(7):4497–503.
85. Frontera P, Macario A, Ferraro M, Antonucci P. Supported catalysts for CO_2 methanation: a review. Catalysts. 2017;7(2):59.
86. Arandiyan H, Wang Y, Sun HY, Rezaei M, Dai HX. Ordered meso- and macroporous perovskite oxide catalysts for emerging applications. Chem Commun. 2018;54(50):6484–502.
87. Arandiyan H, Wang Y, Scott J, Mesgari S, Dai HX, Amal R. In situ exsolution of bimetallic Rh-Ni nanoalloys: a highly efficient catalyst for CO_2 methanation. ACS Appl Mater Interfaces. 2018;10(19):16352–7.
88. Wang Y, Arandiyan H, Scott J, Dai HX, Amal R. Hierarchically porous network-like Ni/Co_3O_4: noble metal-free catalysts for carbon dioxide methanation. Adv Sustain Syst. 2018;2(3):1700119.
89. Chang X, Wang T, Gong J. CO_2 photo-reduction: insights into CO_2 activation and reaction on surfaces of photocatalysts. Energy Environ Sci. 2016;9(7):2177–96.
90. Neațu S, Maciá-Agulló JA, Concepción P, Garcia H. Gold–copper nanoalloys supported on TiO_2 as photocatalysts for CO_2 reduction by water. J Am Chem Soc. 2014;136(45):15969–76.
91. Huang M, Fabris S. CO adsorption and oxidation on ceria surfaces from DFT+U calculations. J Phys Chem C. 2008;112(23):8643–8.
92. Kale MJ, Avanesian T, Xin H, Yan J, Christopher P. Controlling catalytic selectivity on metal nanoparticles by direct photoexcitation of adsorbate–metal bonds. Nano Lett. 2014;14(9):5405–12.
93. Lindstrom C, Zhu X-Y. Photoinduced electron transfer at molecule–metal interfaces. Chem Rev. 2006;106(10):4281–300.
94. Kim C, Hyeon S, Lee J, Kim WD, Lee DC, Kim J, Lee H. Energy-efficient CO_2 hydrogenation with fast response using photoexcitation of CO_2 adsorbed on metal catalysts. Nat Commun. 2018;9(1):3027.
95. Zhu DD, Liu JL, Qiao SZ. Recent advances in inorganic heterogeneous electrocatalysts for reduction of carbon dioxide. Adv Mater. 2016;28(18):3423–52.
96. Singh MR, Clark EL, Bell AT. Effects of electrolyte, catalyst, and membrane composition and operating conditions on the performance of solar-driven electrochemical reduction of carbon dioxide. Phys Chem Chem Phys. 2015;17(29):18924–36.
97. Vasileff A, Zheng Y, Qiao SZ. Carbon solving carbon's problems: recent progress of nanostructured carbon-based catalysts for the electrochemical reduction of CO_2. Adv Eng Mater. 2017;7(21):1700759.
98. Seh ZW, Kibsgaard J, Dickens CF, Chorkendorff IB, Norskov JK, Jaramillo TF. Combining theory and experiment in electrocatalysis: insights into materials design. Science. 2017;355(6321):4998.
99. Bushuyev OS, De Luna P, Dinh CT, Tao L, Saur G, van de Lagemaat J, Kelley SO, Sargent EH. What should we make with CO_2 and how can we make it? Joule. 2018;2(5):825–32.
100. Wang YH, Liu JL, Wang YF, Al-Enizi AM, Zheng GF. Tuning of CO_2 reduction selectivity on metal electrocatalysts. Small. 2017;13(43):1701809.
101. Vasileff A, Xu CC, Jiao Y, Zheng Y, Qiao SZ. Surface and interface engineering in copper-based bimetallic materials for selective CO_2 electroreduction. Chem. 2018;4(8):1809–31.
102. Kuhl KP, Hatsukade T, Cave ER, Abram DN, Kibsgaard J, Jaramillo TF. Electrocatalytic conversion of carbon dioxide to methane and methanol on transition metal surfaces. J Am Chem Soc. 2014;136(40):14107–13.
103. Feaster JT, Shi C, Cave ER, Hatsukade TT, Abram DN, Kuhl KP, Hahn C, Norskov JK, Jaramillo TF. Understanding selectivity for the electrochemical reduction of carbon dioxide to formic acid and carbon monoxide on metal electrodes. ACS Catal. 2017;7(7):4822–7.
104. Hatsukade T, Kuhl KP, Cave ER, Abram DN, Jaramillo TF. Insights into the electrocatalytic reduction of CO_2 on metallic silver surfaces. Phys Chem Chem Phys. 2014;16(27):13814–9.
105. Kim C, Jeon HS, Eom T, Jee MS, Kim H, Friend CM, Min BK, Hwang YJ. Achieving selective and efficient electrocatalytic activity for CO_2 reduction using immobilized silver nanoparticles. J Am Chem Soc. 2015;137(43):13844–50.
106. Zhu WL, Michalsky R, Metin O, Lv HF, Guo SJ, Wright CJ, Sun XL, Peterson AA, Sun SH. Monodisperse Au nanoparticles for selective electrocatalytic reduction of CO_2 to CO. J Am Chem Soc. 2013;135(45):16833–6.
107. Nursanto EB, Jeon HS, Kim C, Jee MS, Koh JH, Hwang YJ, Min BK. Gold catalyst reactivity for CO_2 electro-reduction: from nano particle to layer. Catal Today. 2016;260:107–11.
108. Verma S, Hamasaki Y, Kim C, Huang WX, Lu S, Jhong HRM, Gewirth AA, Fujigaya T, Nakashima N, Kenis PJA. Insights into the low overpotential electroreduction of CO_2 to CO on a supported gold catalyst in an alkaline flow electrolyzer. ACS Energy Lett. 2018;3(1):193–8.
109. Mistry H, Reske R, Zeng ZH, Zhao ZJ, Greeley J, Strasser P, Roldan Cuenya B. Exceptional size-dependent activity enhancement in the electroreduction of CO_2 over Au nanoparticles. J Am Chem Soc. 2014;136(47):16473–6.
110. Yoon Y, Hall AS, Surendranath Y. Tuning of silver catalyst mesostructure promotes selective carbon dioxide conversion into fuels. Angew Chem Int Ed. 2016;55(49):15282–6.
111. Hall AS, Yoon Y, Wuttig A, Surendranath Y. Mesostructure-induced selectivity in CO_2 reduction catalysis. J Am Chem Soc. 2015;137(47):14834–7.
112. Zhu WL, Zhang YJ, Zhang HY, Lv HF, Li Q, Michalsky R, Peterson AA, Sun SH. Active and selective conversion of CO_2 to CO on ultrathin Au nanowires. J Am Chem Soc. 2014;136(46):16132–5.
113. Liu M, Pang YJ, Zhang B, De Luna P, Voznyy O, Xu JX, Zheng XL, Dinh CT, Fan FJ, Cao CH, et al. Enhanced electrocatalytic CO_2 reduction via field-induced reagent concentration. Nature. 2016;537(7620):382.
114. Safaei TS, Mepham A, Zheng XL, Pang YJ, Dinh CT, Liu M, Sinton D, Kelley SO, Sargent EH. High-density nanosharp microstructures enable efficient CO_2 electroreduction. Nano Lett. 2016;16(11):7224–8.
115. Lee HE, Yang KD, Yoon SM, Ahn HY, Lee YY, Chang HJ, Jeong DH, Lee YS, Kim MY, Nam KT. Concave rhombic dodecahedral Au nanocatalyst with multiple high-index facets for CO_2 reduction. ACS Nano. 2015;9(8):8384–93.
116. Kim JH, Woo H, Choi JW, Jung HW, Kim YT. CO_2 electroreduction on Au/TiC: enhanced activity due to metal-support interaction. ACS Catal. 2017;7(3):2101–6.
117. Won DH, Shin H, Koh J, Chung J, Lee HS, Kim H, Woo SI. Highly efficient, selective, and stable CO_2 electroreduction on a hexagonal Zn catalyst. Angew Chem Int Ed. 2016;55(32):9297–300.
118. Rosen J, Hutchings GS, Lu Q, Forest RV, Moore A, Jiao F. Electrodeposited Zn dendrites with enhanced CO selectivity for electrocatalytic CO_2 reduction. ACS Catal. 2015;5(8):4586–91.
119. Quan FJ, Zhong D, Song HC, Jia FL, Zhang LZ. A highly efficient zinc catalyst for selective electroreduction of carbon dioxide in aqueous NaCl solution. J Mater Chem A. 2015;3(32):16409–13.
120. Gao DF, Zhou H, Wang J, Miao S, Yang F, Wang GX, Wang JG, Bao XH. Size-dependent electrocatalytic reduction of CO_2 over Pd nanoparticles. J Am Chem Soc. 2015;137(13):4288–91.
121. Gao DF, Zhou H, Cai F, Wang JG, Wang GX, Bao XH. Pd-containing nanostructures for electrochemical CO_2 reduction reaction. ACS Catal. 2018;8(2):1510–9.
122. Cho M, Song JT, Back S, Jung Y, Oh J. The role of adsorbed CN and Cl on an Au electrode for electrochemical CO_2 reduction. ACS Catal. 2018;8(2):1178–85.
123. Jiang K, Kharel P, Peng YD, Gangishetty MK, Lin HYG, Stavitski E, Attenkofer K, Wang HT. Silver nanoparticles with surface-bonded oxygen for highly selective CO_2 reduction. ACS Sustain Chem Eng. 2017;5(10):8529–34.
124. Kim C, Eom T, Jee MS, Jung H, Kim H, Min BK, Hwang YJ. Insight into electrochemical CO_2 reduction on surface-molecule mediated Ag nanoparticles. ACS Catal. 2017;7(1):779–85.
125. Lee CW, Cho NH, Yang KD, Nam KT. Reaction mechanisms of the electrochemical conversion of carbon dioxide to formic acid on tin oxide electrodes. ChemElectroChem. 2017;4(9):2130–6.
126. Yoo JS, Christensen R, Vegge T, Norskov JK, Studt F. Theoretical insight into the trends that guide the electrochemical reduction of carbon dioxide to formic acid. ChemSusChem. 2016;9(4):358–63.
127. He JF, Johnson NJJ, Huang AX, Berlinguette CP. Electrocatalytic alloys for CO_2 reduction. ChemSusChem. 2018;11(1):48–57.
128. Chen YH, Kanan MW. Tin oxide dependence of the CO_2 reduction efficiency on tin electrodes and enhanced activity for tin/tin oxide thin-film catalysts. J Am Chem Soc. 2012;134(4):1986–9.
129. Zhang S, Kang P, Meyer TJ. Nanostructured tin catalysts for selective electrochemical reduction of carbon dioxide to formate. J Am Chem Soc. 2014;136(5):1734–7.
130. Gu J, Heroguel F, Luterbacher J, Hu XL. Densely packed, ultra small SnO nanoparticles for enhanced activity and selectivity in electrochemical CO_2 reduction. Angew Chem Int Ed. 2018;57(11):2943–7.
131. Kumar B, Atla V, Brian JP, Kumari S, Nguyen TQ, Sunkara M, Spurgeon JM. Reduced SnO_2 porous nanowires with a high density of grain boundaries as

catalysts for efficient electrochemical CO_2-into-HCOOH conversion. Angew Chem Int Ed. 2017;56(13):3645–9.
132. Li FW, Chen L, Knowles GP, MacFarlane DR, Zhang J. Hierarchical mesoporous SnO_2 nanosheets on carbon cloth: a robust and flexible electrocatalyst for CO_2 reduction with high efficiency and selectivity. Angew Chem Int Ed. 2017;56(2):505–9.
133. Won DH, Choi CH, Chung J, Chung MW, Kim EH, Woo SI. Rational design of a hierarchical tin dendrite electrode for efficient electrochemical reduction of CO_2. ChemSusChem. 2015;8(18):3092–8.
134. Zheng XL, De Luna P, de Arquer FPG, Zhang B, Becknell N, Ross MB, Li YF, Banis MN, Li YZ, Liu M, et al. Sulfur-modulated tin sites enable highly selective electrochemical reduction of CO_2 to formate. Joule. 2017;1(4):794–805.
135. Han N, Wang Y, Yang H, Deng J, Wu JH, Li YF, Li YG. Ultrathin bismuth nanosheets from in situ topotactic transformation for selective electrocatalytic CO_2 reduction to formate. Nat Commun. 2018;9:1320.
136. Lee CH, Kanan MW. Controlling H^+ vs CO_2 reduction selectivity on Pb electrodes. ACS Catal. 2015;5(1):465–9.
137. Hara K, Kudo A, Sakata T. Electrochemical reduction of carbon-dioxide under high-pressure on various electrodes in an aqueous-electrolyte. J Electroanal Chem. 1995;391(1–2):141–7.
138. Melchionna M, Bracamonte MV, Giuliani A, Nasi L, Montini T, Tavagnacco C, Bonchio M, Fornasiero P, Prato M. Pd@TiO_2/carbon nanohorn electrocatalysts: reversible CO_2 hydrogenation to formic acid. Energy Environ Sci. 2018;11(6):1571–80.
139. Min XQ, Kanan MW. Pd-catalyzed electrohydrogenation of carbon dioxide to formate: high mass activity at low overpotential and identification of the deactivation pathway. J Am Chem Soc. 2015;137(14):4701–8.
140. Kuhl KP, Cave ER, Abram DN, Jaramillo TF. New insights into the electrochemical reduction of carbon dioxide on metallic copper surfaces. Energy Environ Sci. 2012;5(5):7050–9.
141. Sandberg RB, Montoya JH, Chan K, Norskov JK. CO-CO coupling on Cu facets: coverage, strain and field effects. Surf Sci. 2016;654:56–62.
142. Montoya JH, Peterson AA, Norskov JK. Insights into CC coupling in CO_2 electroreduction on copper electrodes. ChemCatChem. 2013;5(3):737–42.
143. Garza AJ, Bell AT, Head-Gordon M. Mechanism of CO_2 reduction at copper surfaces: pathways to C-2 products. ACS Catal. 2018;8(2):1490–9.
144. Hori Y, Murata A, Takahashi R. Formation of hydrocarbons in the electrochemical reduction of carbon-dioxide at a copper electrode in aqueous-solution. J Chem Soc Faraday Trans 1. 1989;85:2309–26.
145. Peterson AA, Abild-Pedersen F, Studt F, Rossmeisl J, Norskov JK. How copper catalyzes the electroreduction of carbon dioxide into hydrocarbon fuels. Energy Environ Sci. 2010;3(9):1311–5.
146. Huang Y, Handoko AD, Hirunsit P, Yeo BS. Electrochemical reduction of CO_2 using copper single-crystal surfaces: effects of CO* coverage on the selective formation of ethylene. ACS Catal. 2017;7(3):1749–56.
147. Schouten KJP, Kwon Y, van der Ham CJM, Qin Z, Koper MTM. A new mechanism for the selectivity to C-1 and C-2 species in the electrochemical reduction of carbon dioxide on copper electrodes. Chem Sci. 2011;2(10):1902–9.
148. Lum YW, Cheng T, Goddard WA, Ager JW. Electrochemical CO reduction builds solvent water into oxygenate products. J Am Chem Soc. 2018; 140(30):9337–40.
149. Kas R, Kortlever R, Yilmaz H, Koper MTM, Mul G. Manipulating the hydrocarbon selectivity of copper nanoparticles in CO_2 electroreduction by process conditions. ChemElectroChem. 2015;2(3):354–8.
150. Jiang K, Sandberg RB, Akey AJ, Liu XY, Bell DC, Norskov JK, Chan KR, Wang HT. Metal ion cycling of Cu foil for selective C-C coupling in electrochemical CO_2 reduction. Nat Catal. 2018;1(2):111–9.
151. Loiudice A, Lobaccaro P, Kamali EA, Thao T, Huang BH, Ager JW, Buonsanti R. Tailoring copper nanocrystals towards C-2 products in electrochemical CO_2 reduction. Angew Chem Int Ed. 2016;55(19):5789–92.
152. Roberts FS, Kuhl KP, Nilsson A. High selectivity for ethylene from carbon dioxide reduction over copper nanocube electrocatalysts. Angew Chem Int Ed. 2015;54(17):5179–82.
153. Wang ZN, Yang G, Zhang ZR, Jin MS, Yin YD. Selectivity on etching: creation of high-energy facets on copper nanocrystals for CO_2 electrochemical reduction. ACS Nano. 2016;10(4):4559–64.
154. Hori Y, Takahashi I, Koga O, Hoshi N. Selective formation of C2 compounds from electrochemical reduction of CO_2 at a series of copper single crystal electrodes. J Phys Chem B. 2002;106(1):15–7.
155. Sen S, Liu D, Palmore GTR. Electrochemical reduction of CO_2 at copper nanofoams. ACS Catal. 2014;4(9):3091–5.
156. Cao L, Raciti D, Li CY, Livi KJT, Rottmann PF, Hemker KJ, Mueller T, Wang C. Mechanistic insights for low-overpotential electroreduction of CO_2 to CO on copper nanowires. ACS Catal. 2017;7(12):8578–87.
157. Ma M, Djanashvili K, Smith WA. Controllable hydrocarbon formation from the electrochemical reduction of CO_2 over Cu nanowire arrays. Angew Chem Int Ed. 2016;55(23):6680–4.
158. Huang P, Ci SQ, Wang GX, Jia JC, Xu JW, Wen ZH. High-activity Cu nanowires electrocatalysts for CO_2 reduction. J CO2 UTIL. 2017;20:27–33.
159. Raciti D, Livi KJ, Wang C. Highly dense Cu nanowires for low-overpotential CO_2 reduction. Nano Lett. 2015;15(10):6829–35.
160. Ma M, Djanashvili K, Smith WA. Selective electrochemical reduction of CO_2 to CO on CuO-derived Cu nanowires. Phys Chem Chem Phys. 2015;17(32):20861–7.
161. Hoang TTH, Ma SC, Gold JI, Kenis PJA, Gewirth AA. Nanoporous copper films by additive-controlled electrodeposition: CO_2 reduction catalysis. ACS Catal. 2017;7(5):3313–21.
162. Song H, Im M, Song JT, Lim JA, Kim BS, Kwon Y, Ryu S, Oh J. Effect of mass transfer and kinetics in ordered Cu-mesostructures for electrochemical CO_2 reduction. Appl Catal B. 2018;232:391–6.
163. Yang KD, Ko WR, Lee JH, Kim SJ, Lee H, Lee MH, Nam KT. Morphology-directed selective production of ethylene or ethane from CO_2 on a Cu mesopore electrode. Angew Chem Int Ed. 2017;56(3):796–800.
164. De Luna P, Quintero-Bermudez R, Dinh CT, Ross MB, Bushuyev OS, Todorovic P, Regier T, Kelley SO, Yang PD, Sargent EH. Catalyst electro-redeposition controls morphology and oxidation state for selective carbon dioxide reduction. Nat Catal. 2018;1(2):103–10.
165. Rahaman M, Dutta A, Zanetti A, Broekmann P. Electrochemical reduction of CO_2 into multicarbon alcohols on activated Cu mesh catalysts: an identical location (IL) study. ACS Catal. 2017;7(11):7946–56.
166. Jeon HS, Kunze S, Scholten F, Roldan Cuenya B. Prism-shaped Cu nanocatalysts for electrochemical CO_2 reduction to ethylene. ACS Catal. 2018;8(1):531–5.
167. Chung J, Won DH, Koh J, Kim EH, Woo SI. Hierarchical Cu pillar electrodes for electrochemical CO_2 reduction to formic acid with low overpotential. Phys Chem Chem Phys. 2016;18(8):6252–8.
168. Ren D, Deng YL, Handoko AD, Chen CS, Malkhandi S, Yeo BS. Selective electrochemical reduction of carbon dioxide to ethylene and ethanol on copper(I) oxide catalysts. ACS Catal. 2015;5(5):2814–21.
169. Kas R, Kortlever R, Milbrat A, Koper MTM, Mul G, Baltrusaitis J. Electrochemical CO_2 reduction on Cu_2O-derived copper nanoparticles: controlling the catalytic selectivity of hydrocarbons. Phys Chem Chem Phys. 2014;16(24):12194–201.
170. Lee SY, Jung H, Kim NK, Oh HS, Min BK, Hwang YJ. Mixed copper states in anodized Cu electrocatalyst for stable and selective ethylene production from CO_2 reduction. J Am Chem Soc. 2018;140(28):8681–9.
171. Dinh CT, Burdyny T, Kibria MG, Seifitokaldani A, Gabardo CM, de Arquer FPG, Kiani A, Edwards JP, De Luna P, Bushuyev OS, et al. CO_2 electroreduction to ethylene via hydroxide-mediated copper catalysis at an abrupt interface. Science. 2018;360(6390):783–7.
172. Pander JE, Ren D, Huang Y, Loo NWX, Hong SHL, Yeo BS. Understanding the heterogeneous electrocatalytic reduction of carbon dioxide on oxide-derived catalysts. ChemElectroChem. 2018;5(2):219–37.
173. Lee S, Kim D, Lee J. Electrocatalytic production of C3-C4 compounds by conversion of CO_2 on a chloride-induced bi-phasic Cu_2O-Cu catalyst. Angew Chem Int Ed. 2015;54(49):14701–5.
174. Chen YH, Li CW, Kanan MW. Aqueous CO_2 reduction at very low overpotential on oxide-derived Au nanoparticles. J Am Chem Soc. 2012; 134(49):19969–72.
175. Ma M, Trzesniewski BJ, Xie J, Smith WA. Selective and efficient reduction of carbon dioxide to carbon monoxide on oxide-derived nanostructured silver electrocatalysts. Angew Chem Int Ed. 2016;55(33):9748–52.
176. Verdaguer-Casadevall A, Li CW, Johansson TP, Scott SB, McKeown JT, Kumar M, Stephens IEL, Kanan MW, Chorkendorff I. Probing the active surface sites for CO reduction on oxide-derived copper electrocatalysts. J Am Chem Soc. 2015;137(31):9808–11.
177. Feng XF, Jiang KL, Fan SS, Kanan MW. A direct grain-boundary-activity correlation for CO electroreduction on Cu nanoparticles. ACS Cent Sci. 2016;2(3):169–74.
178. Mariano RG, McKelvey K, White HS, Kanan MW. Selective increase in CO_2 electroreduction activity at grain-boundary surface terminations. Science. 2017;358(6367):1187–91.
179. Eilert A, Cavalca F, Roberts FS, Osterwalder J, Liu C, Favaro M, Crumlin EJ, Ogasawara H, Friebel D, Pettersson LGM, et al. Subsurface oxygen in oxide-

derived copper electrocatalysts for carbon dioxide reduction. J Phys Chem Lett. 2017;8(1):285–90.
180. Favaro M, Xiao H, Cheng T, Goddard WA, Yano J, Crumlin EJ. Subsurface oxide plays a critical role in CO_2 activation by Cu (111) surfaces to form chemisorbed CO_2, the first step in reduction of CO_2. Proc Natl Acad Sci U S A. 2017;114(26):6706–11.
181. Lum YW, Ager JW. Stability of residual oxides in oxide-derived copper catalysts for electrochemical CO_2 reduction investigated with O-18 labeling. Angew Chem Int Ed. 2018;57(2):551–4.
182. Clark EL, Hahn C, Jaramillo TF, Bell AT. Electrochemical CO2 reduction over compressively strained CuAg surface alloys with enhanced multi-carbon oxygenate selectivity. J Am Chem Soc. 2017;139(44):15848–57.
183. Kim D, Resasco J, Yu Y, Asiri AM, Yang PD. Synergistic geometric and electronic effects for electrochemical reduction of carbon dioxide using gold-copper bimetallic nanoparticles. Nat Commun. 2014;5:4948.
184. Kim D, Xie CL, Becknell N, Yu Y, Karamad M, Chan K, Crumlin EJ, Norskov JK, Yang PD. Electrochemical activation of CO_2 through atomic ordering transformations of AuCu nanoparticles. J Am Chem Soc. 2017;139(24):8329–36.
185. Ma S, Sadakiyo M, Heima M, Luo R, Haasch RT, Gold JI, Yamauchi M, Kenis PJA. Electroreduction of carbon dioxide to hydrocarbons using bimetallic Cu-Pd catalysts with different mixing patterns. J Am Chem Soc. 2017;139(1):47–50.
186. Hirunsit P, Soodsawang W, Limtrakul J. CO_2 electrochemical reduction to methane and methanol on copper-based alloys: theoretical insight. J Phys Chem C. 2015;119(15):8238–49.
187. Larrazabal GO, Martin AJ, Mitchell S, Hauert R, Perez-Ramirez J. Enhanced reduction of CO_2 to CO over Cu-In electrocatalysts: catalyst evolution is the key. ACS Catal. 2016;6(9):6265–74.
188. Sarfraz S, Garcia-Esparza AT, Jedidi A, Cavallo L, Takanabe K. Cu-Sn bimetallic catalyst for selective aqueous electroreduction of CO_2 to CO. ACS Catal. 2016;6(5):2842–51.
189. Kortlever R, Peters I, Koper S, Koper MTM. Electrochemical CO_2 reduction to formic acid at low overpotential and with high faradaic efficiency on carbon-supported bimetallic Pd-Pt nanoparticles. ACS Catal. 2015;5(7):3916–23.
190. Luc W, Collins C, Wang SW, Xin HL, He K, Kang YJ, Jiao F. Ag-Sn bimetallic catalyst with a core-shell structure for CO_2 reduction. J Am Chem Soc. 2017; 139(5):1885–93.
191. Choi SY, Jeong SK, Kim HJ, Baek IH, Park KT. Electrochemical reduction of carbon dioxide to formate on tin-lead alloys. ACS Sustain Chem Eng. 2016; 4(3):1311–8.
192. Bai XF, Chen W, Zhao CC, Li SG, Song YF, Ge RP, Wei W, Sun YH. Exclusive formation of formic acid from CO_2 electroreduction by a tunable Pd-Sn alloy. Angew Chem Int Ed. 2017;56(40):12219–23.
193. Hahn C, Abram DN, Hansen HA, Hatsukade T, Jackson A, Johnson NC, Hellstern TR, Kuhl KP, Cave ER, Feaster JT, et al. Synthesis of thin film AuPd alloys and their investigation for electrocatalytic CO_2 reduction. J Mater Chem A. 2015;3(40):20185–94.
194. Liu X, Dai LM. Carbon-based metal-free catalysts. Nat Rev Mater. 2016;1(11): 16064.
195. Asefa T. Metal-free and noble metal-free heteroatom-doped nanostructured carbons as prospective sustainable electrocatalysts. Acc Chem Res. 2016; 49(9):1873–83.
196. Duan XC, Xu JT, Wei ZX, Ma JM, Guo SJ, Wang SY, Liu HK, Dou SX. Metal-free carbon materials for CO_2 electrochemical reduction. Adv Mater. 2017; 29(41):1701784.
197. Guo DH, Shibuya R, Akiba C, Saji S, Kondo T, Nakamura J. Active sites of nitrogen-doped carbon materials for oxygen reduction reaction clarified using model catalysts. Science. 2016;351(6271):361–5.
198. Liu S, Yang HB, Huang X, Liu LH, Cai WZ, Gao JJ, Li XN, Zhang T, Huang YQ, Liu B. Identifying active sites of nitrogen-doped carbon materials for the CO_2 reduction reaction. Adv Funct Mater. 2018;28(21):1800499.
199. Xu JY, Kan YH, Huang R, Zhang BS, Wang BL, Wu KH, Lin YM, Sun XY, Li QF, Centi G, et al. Revealing the origin of activity in nitrogen-doped nanocarbons towards electrocatalytic reduction of carbon dioxide. ChemSusChem. 2016;9(10):1085–9.
200. Wu JJ, Yadav RM, Liu MJ, Sharma PP, Tiwary CS, Ma LL, Zou XL, Zhou XD, Yakobson BI, Lou J, et al. Achieving highly efficient, selective, and stable CO_2 reduction on nitrogen-doped carbon nanotubes. ACS Nano. 2015;9(5):5364–71.
201. Sharma PP, Wu JJ, Yadav RM, Liu MJ, Wright CJ, Tiwary CS, Yakobson BI, Lou J, Ajayan PM, Zhou XD. Nitrogen-doped carbon nanotube arrays for high-efficiency electrochemical reduction of CO_2: on the understanding of defects, defect density, and selectivity. Angew Chem Int Ed. 2015;54(46): 13701–5.
202. Wu JJ, Liu MJ, Sharma PP, Yadav RM, Ma LL, Yang YC, Zou XL, Zhou XD, Vajtai R, Yakobson BI, et al. Incorporation of nitrogen defects for efficient reduction of CO_2 via two-electron pathway on three-dimensional graphene foam. Nano Lett. 2016;16(1):466–70.
203. Wu JJ, Ma SC, Sun J, Gold JI, Tiwary C, Kim B, Zhu LY, Chopra N, Odeh IN, Vajtai R, et al. A metal-free electrocatalyst for carbon dioxide reduction to multi-carbon hydrocarbons and oxygenates. Nat Commun. 2016;7:13869.
204. Liu YM, Chen S, Quan X, Yu HT. Efficient electrochemical reduction of carbon dioxide to acetate on nitrogen-doped nanodiamond. J Am Chem Soc. 2015;137(36):11631–6.
205. Li WL, Seredych M, Rodriguez-Castellon E, Bandosz TJ. Metal-free nanoporous carbon as a catalyst for electrochemical reduction of CO_2 to CO and CH_4. ChemSusChem. 2016;9(6):606–16.
206. Sreekanth N, Nazrulla MA, Vineesh TV, Sailaja K, Phani KL. Metal-free boron-doped graphene for selective electroreduction of carbon dioxide to formic acid/formate. Chem Commun. 2015;51(89):16061–4.
207. Kim J, Kim HE, Lee H. Single-atom catalysts of precious metals for electrochemical reactions. ChemSusChem. 2018;11(1):104–13.
208. Yang S, Kim J, Tak YJ, Soon A, Lee H. Single-atom catalyst of platinum supported on titanium nitride for selective electrochemical reactions. Angew Chem Int Ed. 2016;55(6):2058–62.
209. Choi CH, Kim M, Kwon HC, Cho SJ, Yun S, Kim HT, Mayrhofer KJJ, Kim H, Choi M. Tuning selectivity of electrochemical reactions by atomically dispersed platinum catalyst. Nat Commun. 2016;7:10922.
210. Deng J, Li HB, Xiao JP, Tu YC, Deng DH, Yang HX, Tian HF, Li JQ, Ren PJ, Bao XH. Triggering the electrocatalytic hydrogen evolution activity of the inert two-dimensional MoS2 surface via single-atom metal doping. Energy Environ Sci. 2015;8(5):1594–601.
211. Kim J, Roh CW, Sahoo SK, Yang S, Bae J, Han JW, Lee H. Highly durable platinum single-atom alloy catalyst for electrochemical reactions. Adv Eng Mater. 2018;8(1):1701476.
212. Yang HB, Hung SF, Liu S, Yuan KD, Miao S, Zhang LP, Huang X, Wang HY, Cai WZ, Chen R, et al. Atomically dispersed Ni(i) as the active site for electrochemical CO_2 reduction. Nat Energy. 2018;3(2):140–7.
213. Jiang K, Siahrostami S, Zheng TT, Hu YF, Hwang S, Stavitski E, Peng YD, Dynes J, Gangisetty M, Su D, et al. Isolated Ni single atoms in graphene nanosheets for high-performance CO_2 reduction. Energy Environ Sci. 2018;11(4):893–903.
214. Jiang K, Siahrostami S, Akey AJ, Li YB, Lu ZY, Lattimer J, Hu YF, Stokes C, Gangishetty M, Chen GX, et al. Transition-metal single atoms in a graphene shell as active centers for highly efficient artificial photosynthesis. Chem. 2017;3(6):950–60.
215. Wang YF, Chen Z, Han P, Du YH, Gu ZX, Xu X, Zheng GF. Single-atomic Cu with multiple oxygen vacancies on ceria for electrocatalytic CO_2 reduction to CH_4. ACS Catal. 2018;8(8):7113–9.
216. Backs S, Jung YS. TiC- and TiN-supported single-atom catalysts for dramatic improvements in CO_2 electrochemical reduction to CH_4. ACS Energy Lett. 2017;2(5):969–75.
217. Back S, Lim J, Kim NY, Kim YH, Jung Y. Single-atom catalysts for CO_2 electroreduction with significant activity and selectivity improvements. Chem Sci. 2017;8(2):1090–6.
218. Cheng MJ, Clark EL, Pham HH, Bell AT, Head-Gordon M. Quantum mechanical screening of single-atom bimetallic alloys for the selective reduction of CO_2 to C-1 hydrocarbons. ACS Catal. 2016;6(11):7769–77.
219. Varela AS, Kroschel M, Reier T, Strasser P. Controlling the selectivity of CO_2 electroreduction on copper: the effect of the electrolyte concentration and the importance of the local pH. Catal Today. 2016;260:8–13.
220. Resasco J, Chen LD, Clark E, Tsai C, Hahn C, Jaramillo TF, Chan K, Bell AT. Promoter effects of alkali metal cations on the electrochemical reduction of carbon dioxide. J Am Chem Soc. 2017;139(32):11277–87.
221. Singh MR, Kwon Y, Lum Y, Ager JW, Bell AT. Hydrolysis of electrolyte cations enhances the electrochemical reduction of CO_2 over Ag and Cu. J Am Chem Soc. 2016;138(39):13006–12.
222. Verma S, Lu X, Ma SC, Masel RI, Kenis PJA. The effect of electrolyte composition on the electroreduction of CO_2 to CO on Ag based gas diffusion electrodes. Phys Chem Chem Phys. 2016;18(10):7075–84.
223. Rosen BA, Salehi-Khojin A, Thorson MR, Zhu W, Whipple DT, Kenis PJA, Masel RI. Ionic liquid-mediated selective conversion of CO_2 to CO at low overpotentials. Science. 2011;334(6056):643–4.

224. Asadi M, Kim K, Liu C, Addepalli AV, Abbasi P, Yasaei P, Phillips P, Behranginia A, Cerrato JM, Haasch R, et al. Nanostructured transition metal dichalcogenide electrocatalysts for CO_2 reduction in ionic liquid. Science. 2016;353(6298):467–70.
225. Cole EB, Lakkaraju PS, Rampulla DM, Morris AJ, Abelev E, Bocarsly AB. Using a one-electron shuttle for the multielectron reduction of CO_2 to methanol: kinetic, mechanistic, and structural insights. J Am Chem Soc. 2010;132(33): 11539–51.
226. Han ZJ, Kortlever R, Chen HY, Peters JC, Agapie T. CO_2 reduction selective for C≥2 products on polycrystalline copper with N-substituted pyridinium additives. ACS Cent Sci. 2017;3(8):853–9.
227. Kim B, Hillman F, Ariyoshi M, Fujikawa S, Kenis PJA. Effects of composition of the micro porous layer and the substrate on performance in the electrochemical reduction of CO_2 to CO. J Power Sources. 2016;312:192–8.

Ready to submit your research? Choose BMC and benefit from:

- fast, convenient online submission
- thorough peer review by experienced researchers in your field
- rapid publication on acceptance
- support for research data, including large and complex data types
- gold Open Access which fosters wider collaboration and increased citations
- maximum visibility for your research: over 100M website views per year

At BMC, research is always in progress.

Learn more biomedcentral.com/submissions

BMC